1-1-2005

Mechanisms of climate variability

Edward A. Bryant
University of Wollongong, ebryant@uow.edu.au

Mechanisms of climate variability

Abstract

Climatic hazards originate with the processes that move air across the Earth's surface due to differential heating and cooling. Surprisingly, examination of these processes has focused upon heating at the tropics and downplayed the role of cold air masses moving out of polar regions due to deficits in the radiation balance in these latter regions. Fluctuations – in the intensity of pulses of cold air moving out of polar regions or of heating at the equator – and the location of the interaction between these cold and warm air masses, are crucial factors in determining the magnitude, frequency, and location of mid-latitude storm systems. While most of these factors are dictated by internal factors in the Earth–atmosphere system, modulation by 11-year geomagnetic cycles linked to solar activity and by the 18.6 year *MN lunar tide* also occurs. This chapter examines these processes and mechanisms. The responses in terms of centers of storm activity will be examined in the following chapter.

Keywords

Mechanisms, Climate, Variability

Disciplines

Life Sciences | Physical Sciences and Mathematics | Social and Behavioral Sciences

Publication Details

Bryant, E. A. (2005). Mechanisms of climate variability. In E. A. Bryant (Eds.), Natural Hazards (pp. 17-43). Port Melbourne, Victoria: Cambridge University Press.

Mechanisms of Climate Variability

CHAPTER 2

INTRODUCTION

Climatic hazards originate with the processes that move air across the Earth's surface due to differential heating and cooling. Surprisingly, examination of these processes has focused upon heating at the tropics and downplayed the role of cold air masses moving out of polar regions due to deficits in the radiation balance in these latter regions. Fluctuations – in the intensity of pulses of cold air moving out of polar regions or of heating at the equator – and the location of the interaction between these cold and warm air masses, are crucial factors in determining the magnitude, frequency, and location of mid-latitude storm systems. While most of these factors are dictated by internal factors in the Earth–atmosphere system, modulation by 11-year geomagnetic cycles linked to solar activity and by the 18.6 year M_N *lunar tide* also occurs. This chapter examines these processes and mechanisms. The responses in terms of centers of storm activity will be examined in the following chapter.

MODELS OF ATMOSPHERIC CIRCULATION AND CHANGE

(Bryson & Murray, 1977; Lamb, 1982)

How air moves

Barometric pressure represents the weight of air above a location on the Earth's surface. When the weight of air over an area is greater than over adjacent areas, it is termed 'high pressure'. When the weight of air is lower, it is termed 'low pressure'. Points of equal pressure across the Earth's surface can be contoured using *isobars*, and on weather maps contouring is generally performed at intervals of 4 *hectopascals* (hPa) or millibars (mb). Mean pressure for the Earth is 1013.6 hPa. Wind is generated by air moving from high to low pressure simply because a pressure gradient exists owing to the difference in air density (Figure 2.1): the stronger the pressure gradient, the stronger the wind. This is represented graphically on weather maps by relatively closely spaced isobars. In reality, wind does not flow down pressure gradients but blows almost parallel to isobars at the surface of the Earth because of *Coriolis force* (Figure 2.1). This force exists because of the rotation of the Earth and is thus illusionary. For example, a person standing perfectly still at the pole would appear to an observer viewing the Earth from the Moon to turn around in a complete circle every

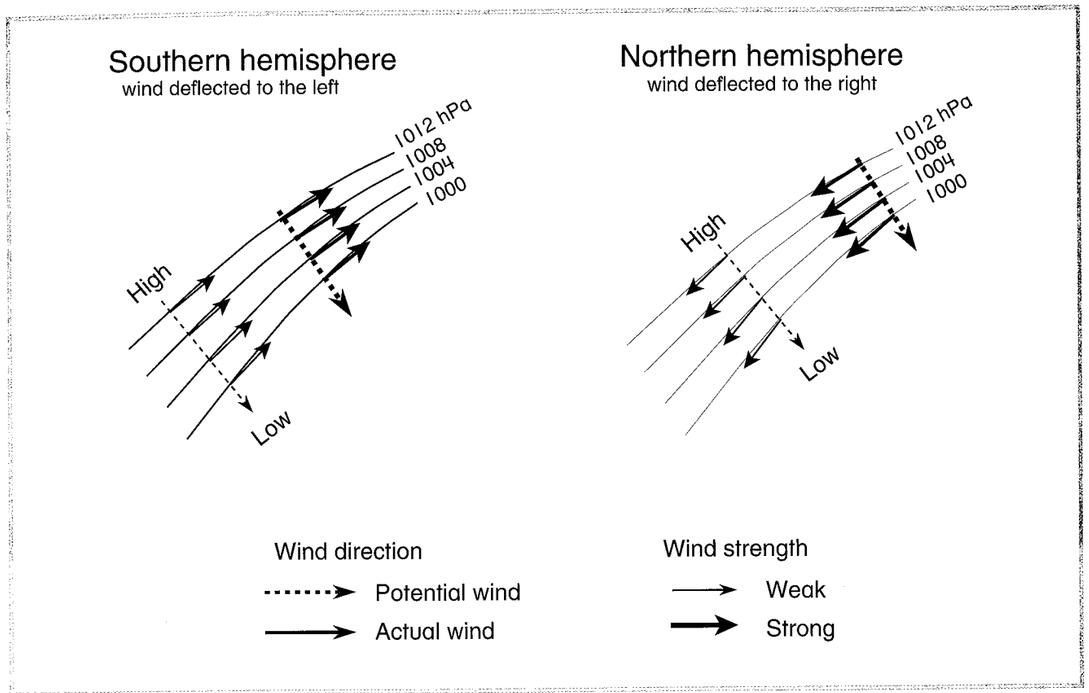

Fig. 2.1 Wind movements relative to isobars, with and without Coriolis force (i.e. potential and actual).

24 hours as the Earth rotates. However, a person standing perfectly still at the equator would always appear to be facing the same direction and not turning around. Because of Coriolis force, wind tends to be deflected to the left in the southern hemisphere and to the right in the northern hemisphere. Coriolis force can be expressed mathematically by the following equation:

$$\text{Coriolis force} = 2\,\omega \sin\phi v \qquad 2.1$$

where ω = rate of spin of the Earth
$\sin \phi$ = latitude
v = wind speed

Clearly, the stronger the pressure gradient, the stronger the wind and the more wind will tend to be deflected. This deflection forms a *vortex*. Also, the stronger the wind, the smaller and more intense is the resulting vortex. Very strong vortices are known as hurricanes, typhoons, cyclones, and tornadoes. Coriolis force varies across the surface of the globe because of latitude and wind velocity. Coriolis force is zero at the equator (sin 0° = 0), and maximum at the pole (sin 90° = 1). The equator is a barrier to inter-hemispheric movement of storms because vortices rotate in opposite directions in each hemisphere. For example, tropical cyclones cannot cross the equator because they rotate clockwise in the southern hemisphere and anti-clockwise in the northern hemisphere.

Palmén–Newton model of global circulation

Upward movement of air is a prerequisite for vortex development, with about 10 per cent of all air movement taking place vertically. As air rises, it spirals because of Coriolis force, and draws in adjacent air at the surface. Rising air is unstable if it is warmer than adjacent air, and instability is favored if *latent heat* can be released through condensation. The faster air rises, the greater the velocity of surface winds spiraling into the center of the vortex. Of course, in the opposite manner, descending air spirals outward at the Earth's surface. These concepts can be combined to account for air movement in the *troposphere*. The Palmén–Newton *general air circulation* model is one of the more thorough models in this regard (Figure 2.2). Intense heating by the sun, at the equator, causes air to rise and spread out poleward in the upper troposphere. As this air moves towards the poles, it cools through long wave

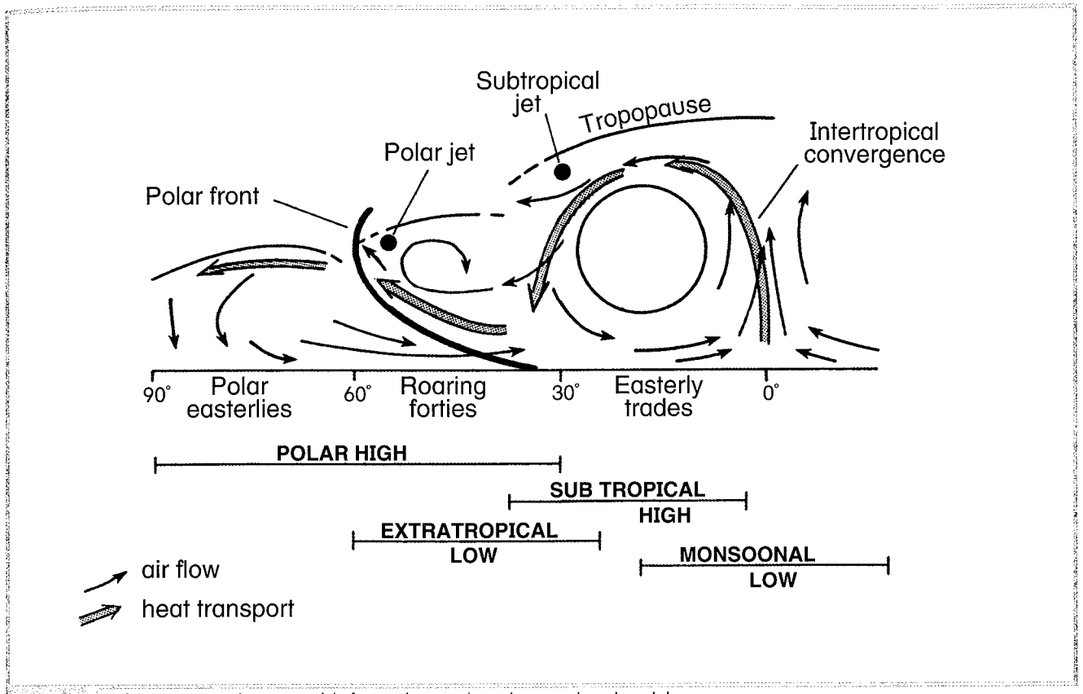

Fig. 2.2 Palmén–Newton schematic model of general air circulation between the pole and the equator.

emission and begins to descend back to the Earth's surface around 20–30° north and south of the solar equator, forming high pressure at the ground. Upon reaching the Earth's surface, this air either moves poleward or returns to the equator to form a closed circulation cell, termed a *Hadley cell*. Because of Coriolis force, equatorial moving air forms two belts of easterly *trade winds* astride the equator. Air tends to converge towards the solar equator, and the uplift zone here is termed the intertropical convergence. Over the western sides of oceans, the tropical easterlies pile up warm water, resulting in *convection* of air that forms low pressure and intense instability. In these regions, intense vortices known as *tropical cyclones* develop preferentially. These will be described in Chapter 3.

At the poles, air cools and spreads along the Earth's surface towards the equator. Where cold polar air meets relatively warmer, subtropical air at mid-latitudes, a cold *polar front* develops with strong uplift and instability. Tornadoes and strong westerlies can be generated near the polar front over land, while intense extra-tropical storms develop near the polar front, especially over water bodies. Tornadoes will be described in Chapter 4, while extra-tropical storms are described in the next chapter. A belt of strong wind and storms – dominated by westerlies poleward of the polar front – forms around 40° latitude in each hemisphere. These winds, known as the roaring forties, are especially prominent in the southern hemisphere where winds blow unobstructed by land or, more importantly, by significant mountain ranges. Maps of global winds support these aspects of the Palmén–Newton model (Figure 2.3).

The Palmén–Newton model has two limitations. First, the location of pressure cells within the model is based upon averages over time. Second, because the model averages conditions, it tends to be static, whereas the Earth's atmosphere is very dynamic. Additionally, the concept of Hadley circulation is overly simplistic. In fact, rising air in the tropics is not uniform, but confined almost exclusively to narrow updrafts within thunderstorms. At higher latitudes, large-scale circulation is distorted by relatively small eddies. Other factors also control winds. For example, over the Greenland or Antarctic icecaps, enhanced radiative cooling forms large pools of cold air, which can accelerate downslope under gravity because of the low *frictional* coefficient of ice. Alternative models that overcome some of these limitations will be presented.

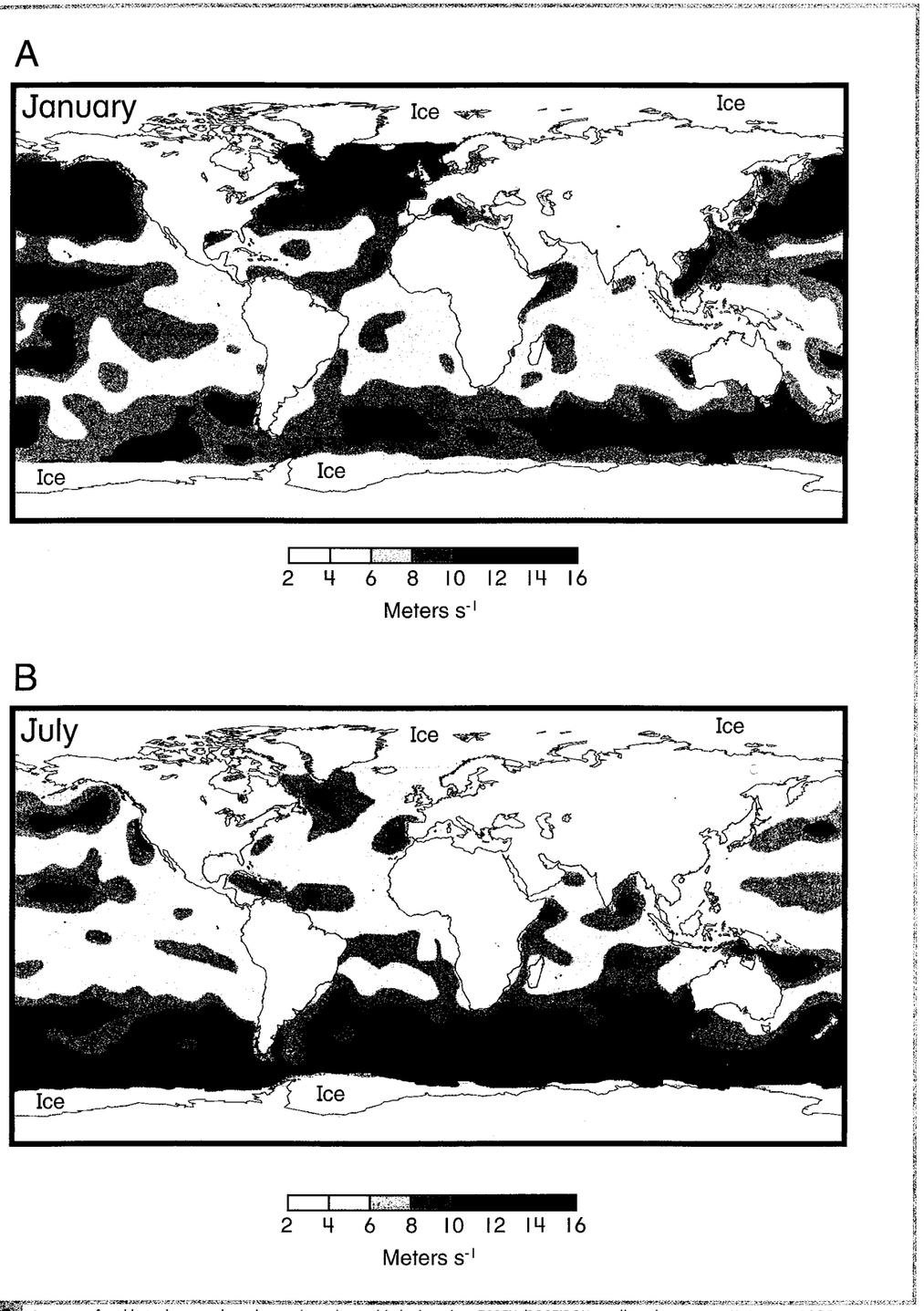

Fig. 2.3 Location of mid-latitude westerly and easterly trade wind belts based on TOPEX/POSEIDON satellite observations A) January 1995, B) July 1995 (Jet Propulsion Laboratory, 1995a, b).

Changes in jet stream paths

Strong winds exist in the upper atmosphere adjacent to the *tropopause* boundary (Figure 2.2). The more significant of these is the polar *jet stream* on the equatorial side of the polar front. This jet stream consists of a zone of strong winds no more than 1 km deep and 100 km wide, flowing downwind over a distance of 1000 km or more. Wind speeds can reach in excess of 250 km hr^{-1}. The polar jet stream is most prominent and continuous in the northern hemisphere. Here, it forms over the Tibetan Plateau, where its position is linked with the seasonal onset and demise of the Indian *monsoon*. The jet loops northward over Japan and is deflected north by the Rocky Mountains. It then swings south across the Great Plains of the United States, north-eastward (parallel to the Appalachian Mountains), and exits North America off Newfoundland, dissipating over Iceland. Both the Tibetan Plateau and the Rocky Mountains produce a resonance effect in wave patterns in the northern hemisphere, locking high pressure cells over Siberia and North America with an intervening low pressure cell over the north Pacific Ocean. Barometric pressure, measured along the 60°N parallel of latitude through these cells, reveals a quasi-stable planetary or *Rossby wave*.

In the northern hemisphere, the jet stream tends to form three to four Rossby waves extending through 5–10° of latitude around the globe (Figure 2.4). Rossby waves move a few hundred kilometres an hour faster than the Earth rotates and thus appear to propagate from west to east. Any disturbance in a Rossby wave thus promulgates downwind, such that a change in weather in North America appears over Europe several days afterwards. This aspect gives *coherence* to extreme events in weather across the northern hemisphere. Because there is a time lag in changes to Rossby waves downwind from North America, forecasters can predict extreme events over Europe days in advance. In some winters, the waves undergo amplification and loop further north and south than normal. Many researchers believe that changes in this looping are responsible, not only for short-term drought (or rainfall), but also for semi-permanent climatic change in a region extending from China to Europe. Sometimes the looping is so severe that winds in the jet stream simply take the path of least resistance, and proceed *zonally* (parallel to latitude), cutting off the loop. In this case, high and low pressure cells can be left stranded in location for days or weeks, unable to be shifted east by the prevailing westerly airflow. High-pressure cells are particularly vulnerable to this process and form *blocking highs*. Blocking highs deflect frontal lows to higher or lower latitudes than normally expected, producing extremes in weather. Blocking is more characteristic of winter, especially in the northern hemisphere. It also tends to occur over abnormally warm seas, on the western sides of oceans.

Expansion of the westerlies because of enhanced looping of Rossby waves can be linked to recent failure

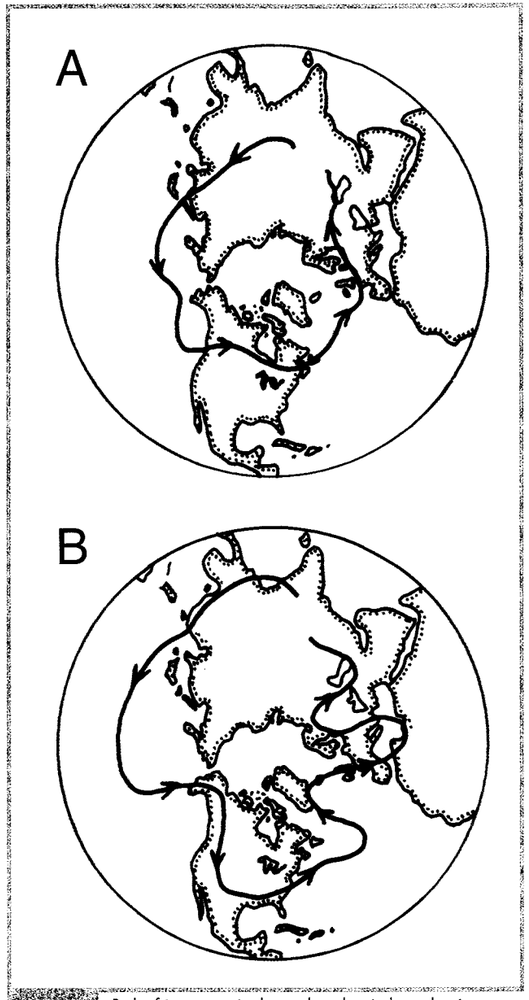

Fig. 2.4 Path of jet stream in the northern hemisphere showing likely Rossby wave patterns A) for summer, B) for extreme winter (Bryson & Murray, ©1977 with the permission of The University of Wisconsin Press).

of monsoon rains and resulting drought in the *Sahel* in the early 1970s. In the Sahara region, rain normally falls as the *intertropical convergence* moves seasonally northward. If westerlies expand, then such movement of the intertropical convergence is impeded and drought conditions prevail. Drought in Britain can also be linked to displacement northward of the jet stream and polar-front lows – shifting into the Arctic instead of crossing Scotland and Norway. This displacement leaves Britain under the influence of an extension of the Azores high-pressure system that is stable and rainfall-deficient. Blocking of this high leads to drought for several months. Blocking highs off the Californian coast were also responsible for drought in the mid-United States in 1997, while highs over eastern Australia have led to some of the worst droughts in that continent's recorded history. The social response to these types of droughts will be examined in Chapter 5.

Mobile polar highs (Leroux, 1993, 1998; Bryant, 1997)

The monsoonal circulation described above does not fit well within the Palmén–Newton general circulation model. In fact, the positioning of Hadley cells, and the semi-permanency of features such as the Icelandic or Aleutian Lows, are statistical artefacts. There is not an Icelandic Low, locked into position over Iceland. Nor are there consistent trades or polar easterlies. Air circulation across the surface of the Earth is dynamic, as is the formation and demise of pressure cells. In reality, the Icelandic Low may exist as an intense cell of low pressure for several days, and then move eastward towards Europe within the westerly air stream. Climate change in the Palmén–Newton model implies the movement, or change in magnitude, of these centers of activity. For example, weakening of the Icelandic Low conveys the view that winter circulation is less severe, while expansion of Hadley cells towards higher latitudes suggests that droughts should dominate mid-latitudes.

There are other problems with terminology in the Palmén–Newton model; these have an historical basis. The depression, extra-tropical cyclone, or polar low was initially explained as a thermal phenomenon, and then linked to frontal uplift along the polar front, to upper air disturbances, and recently to planetary waves or Rossby waves. The jet stream is supposedly tied to the polar front, and related to *cyclogenesis* at mid-latitudes. However, the connection between the jet stream and the polar front is approximate, and a clear relationship has not been established between the jet stream in the upper troposphere and the formation of low pressure at the Earth's surface. Indeed, no one theory adequately explains the initial formation of lows at mid-latitudes. The Palmén–Newton general circulation model is a good teaching model, but it is not an ideal model for explaining the causes of climate change.

Conceptually, the Palmén–Newton model in its simplest form has two areas of forcing: upward air movement at the equator from heating of the Earth's surface, and sinking of air at the poles because of intense cooling caused by long wave emission. At the equator, air moves from higher latitudes to replace the uplifted air, while at the poles subsiding air moves towards the equator as a cold dense mass hugging the Earth's surface. The lateral air movement at the equator is slow and weak, while that at the poles is strong and rapid. Polar surging can reach within 10° of the equator, such that some of the lifting of air in this region can be explained by the magnitude and location of polar outbursts. Hence, the dominant influence on global air circulation lies with outbursts of cold air within polar high-pressure cells. Each of these outbursts forms an event termed a *mobile polar high*. There is no separate belt of high pressure or Hadley cell in the subtropics. These cells, as they appear on synoptic maps, are simply statistical averages over time of the preferred pathways of polar air movement towards the equator.

Mobile polar highs developing in polar regions are initially maintained in position by surface cooling, air subsidence and advection of warm air at higher altitudes. When enough cold air accumulates, it suddenly moves away from the poles, forming a 1500 m thick lens of cold air. In both hemispheres, polar high outbreaks tend to move from west to east, thus conserving vorticity. Additionally, in the southern hemisphere, pathways and the rate of movement are aided by the formation of *katabatic winds* off the Antarctic icecap (Figure 2.5). In the northern hemisphere, outburst pathways are controlled by topography with mobile polar highs tending to occur over the Hudson Bay lowland, Scandinavia and the Bering Sea (Figure 2.5). The distribution of oceans and continents, with their attendant mountains, explains why the mean trajectories followed by these highs are always the same. For instance, over Australia, a polar outbreak always

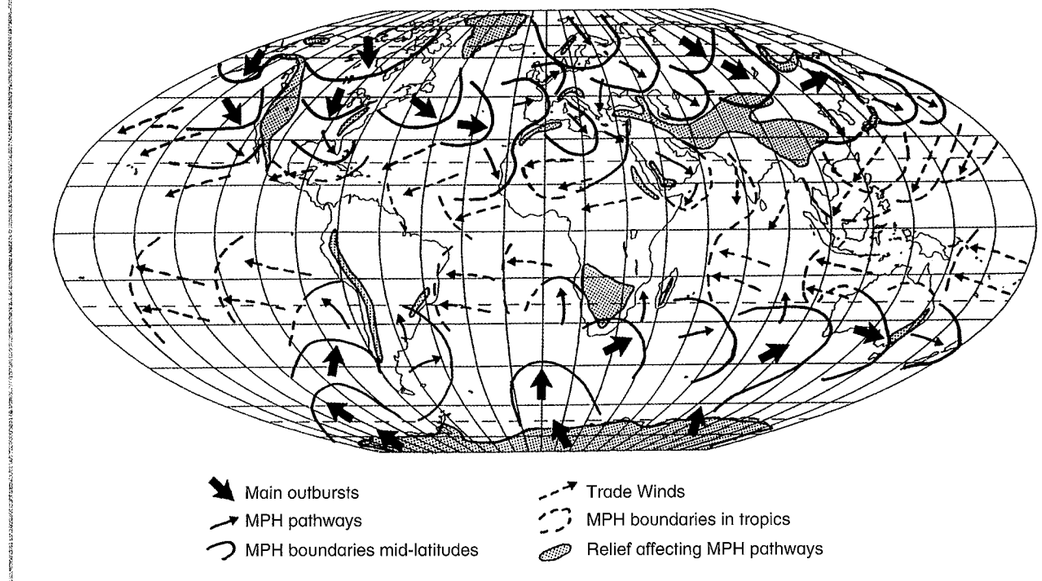

Fig. 2.5 Pathways for mobile polar highs (MPH) and resulting trade wind circulation in the tropics (based on Leroux, 1993).

approaches the continent from the southwest, and then loops across the continent towards the equator, and drifts in the Hadley belt out into the Tasman Sea. Highs rarely move directly northward across the continent, or sweep up from the Tasman Sea. In North America, mobile polar highs regularly surge southward across the Great Plains for the same reason.

Because mobile polar highs consist of dense air, they deflect less dense, warm air upward and to the side. The deflection is greatest in the direction they are moving. Hence, the polar high develops an extensive bulbous, high-pressure vortex, surrounded downdrift by a cyclonic branch or low-pressure cell (Figure 2.6). Typically, the high-pressure cell is bounded by an arching, polar cold front with a low pressure cell attached to the leading edge. However, in the northern hemisphere, individual outbreaks tend to overlap so that the low-pressure vortex becomes contained between two highs. This forms the classic V-shaped, wedged frontal system associated with *extratropical lows or depressions* (Figure 2.6). Thus lows, and upper westerly jet streams, are a product of the displacement and divergence of a mobile polar high. The intensity of the low-pressure cell becomes dependent upon the strength of the polar high, and upon its ability to displace the surrounding air. Strong polar highs produce deep lows; weak highs generate weak lows. In a conceptual sense, a deeper Icelandic or Aleutian Low must be associated with a stronger mobile polar high. If a mobile polar high is particularly cold, it can cause the air above to cool and settle. This creates low pressure above the center of the high-pressure cell, which can develop into a trough and then a cell as upper air flows inwards. If a mobile polar high has lost its momentum and stalled forming a 'blocking high', the low-pressure cell can intensify, propagate to the ground, and generate a surface storm. This process occurs most often on the eastern sides of continents adjacent to mountain ranges such as the Appalachians in the United States and the Great Dividing Range in Australia. These storms will be discussed further in the next chapter.

Mobile polar highs tend to lose their momentum and stack up or *agglutinate* at particular locations over the oceans. A blocking high is simply a stagnant mobile polar high. Air pressure averaged over time thus produces the illusion of two stable, tropical high-pressure belts – known as Hadley cells – on each side of the equator. Mobile polar highs can propagate into the tropics, especially in winter. Here, their arrival tends to intensify the easterly trade winds. More important, yet little realized, is the fact that strong

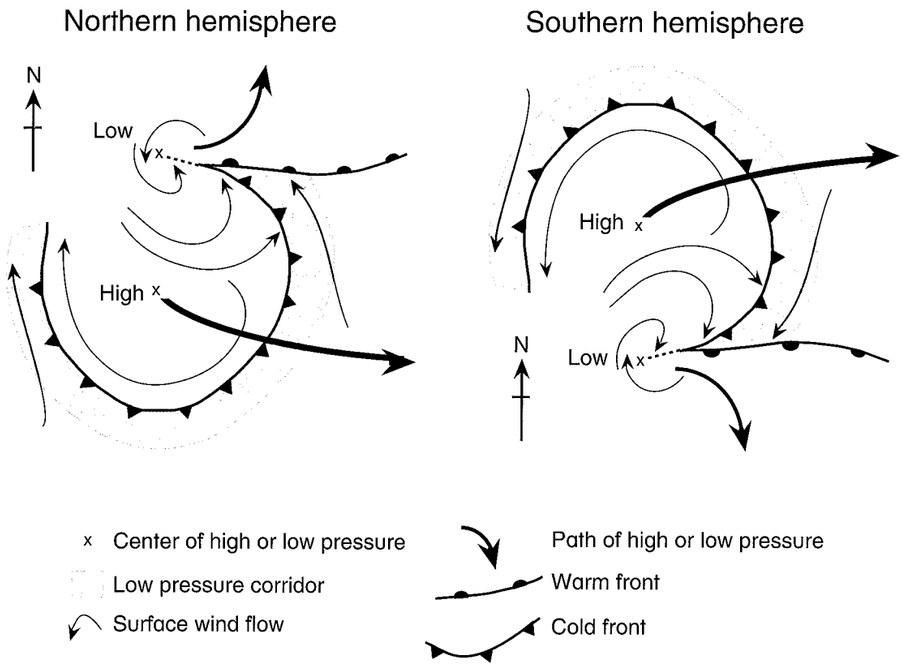

Fig. 2.6 Schematic view of the dynamic structure of a mobile polar high and its associated mid-latitude low (based on Leroux, 1993).

polar highs produce stronger monsoons, although in a more restricted tropical belt.

The Southern Oscillation

Introduction

The Earth's general atmospheric circulation in the tropics and subtropics, as shown above, can be simply described. However, the actual scene is slightly more complex. The intensity of mobile polar highs within a hemisphere varies annually with the apparent movement of the sun north and south of the equator. There is also a subtle, but important, shift in the intensity of heating near the equator. In the northern hemisphere summer, heating shifts from equatorial regions to the Indian mainland with the onset of the Indian monsoon. Air is sucked into the Indian subcontinent from adjacent oceans and landmasses, to return via upper air movement, to either southern Africa or the central Pacific. In the northern hemisphere winter, this intense heating area shifts to the Indonesian–northern Australian 'maritime' continent (Figure 2.7A), with air then moving in the upper troposphere, to the east Pacific. Convection is so intense that updrafts penetrate the tropopause into the *stratosphere*, mainly through *supercell thunderstorms*. These convective cells are labeled *stratospheric fountains*.

Throughout the year, mobile polar highs tend to stack up over the equatorial ocean west of South America. The center of average high pressure here shifts seasonally less than 5° in latitude. The highs are locked into position by positive *feedback*. Cold water in the eastern Pacific Ocean creates high pressure that induces easterly airflow; this process causes upwelling of cold water along the coast, which cools the air. On the western Pacific side, easterlies pile up warm water, thus enhancing *convective instability*, causing air to rise, and perpetuating low pressure. Air is thus continually flowing across the Pacific, as an easterly trade wind from high pressure to low pressure. This circulation is zonal in contrast to the *meridional airflow* inherent within the Palmén–Newton general circulation model. The persistent easterlies blow warm surface water across the Pacific Ocean, piling it up in

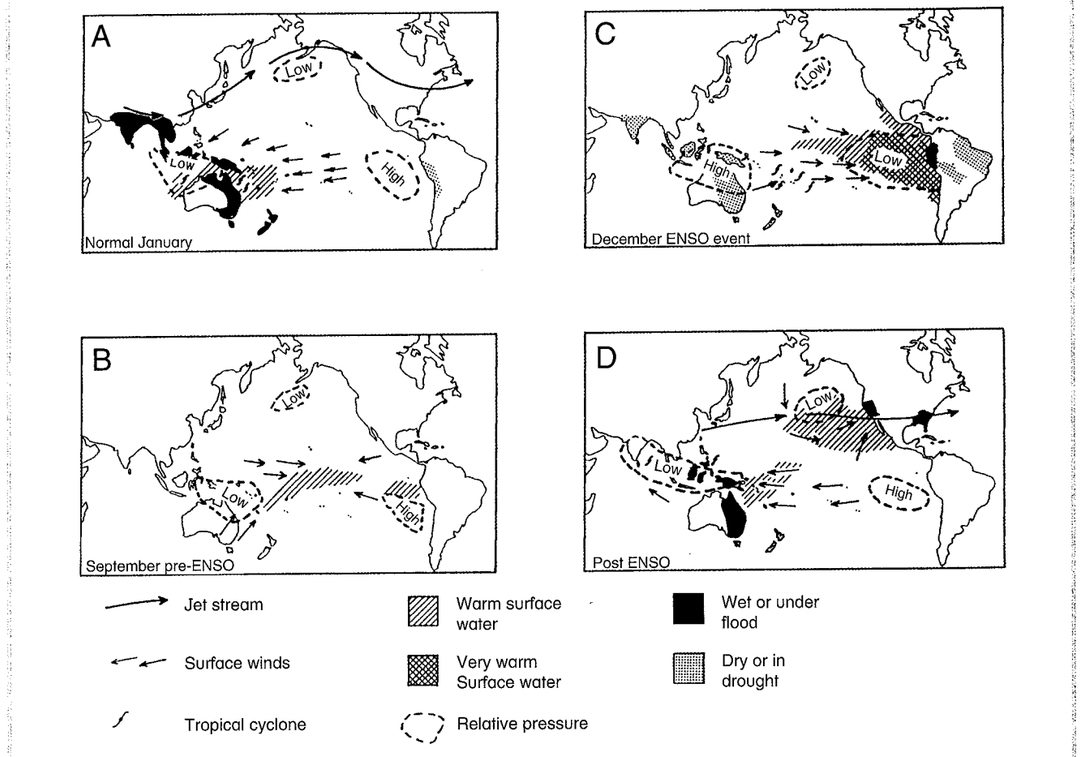

Fig. 2.7 Idealized representation of evolution and effects of an El Niño–Southern Oscillation event.

the west Pacific warm pool in the Philippine Sea. The supra-elevation of sea level in the west Pacific Ocean is approximately 1 cm for each 1°C difference in temperature between the west Pacific and the South American coast. Normally this supra-elevation amounts to 13–20 cm.

This atmospheric system is very stable, existing beyond the annual climatic cycle. The easterly trade wind flow is termed *Walker circulation*, after the Indian meteorologist, Gilbert Walker, who described the phenomenon in detail in the 1920s–1930s. For some inexplicable reason, this quasi-stationary heating process weakens in intensity, or breaks down completely, every 3–5 years – a frequency very suggestive of a chaotic system. High pressure can become established over the Indonesian–Australian area, while low pressure develops over warm water off the South American coast. In the tropics, the easterly winds abate and are replaced by westerly winds. The rainfall belt shifts to the central Pacific and drought replaces normal or heavy rainfall in Australia. Such conditions persisted in the Great World Drought of 1982–1983, which affected most of Australia, Indonesia, India, and South Africa.

Because it tends to fluctuate, this phenomenon is called the *Southern Oscillation* (SO). Simply subtracting the barometric pressure for Darwin from that of Tahiti produces an index of the intensity and fluctuations of the SO. This value is then *normalized* to a mean of 0.0 hPa and a standard deviation of 10. This normalized index, from 1851 to the present, is presented in Figure 2.8.

Warm water usually appears (albeit in reduced amounts) along the Peruvian coast around Christmas each year. This annual warming is termed the *El Niño*, which is Spanish for 'Christ Child'. However, when Walker circulation collapses, this annual warming becomes exaggerated, with sea surface temperatures increasing 4–6°C above normal and remaining that way for several months. This localized, above average,

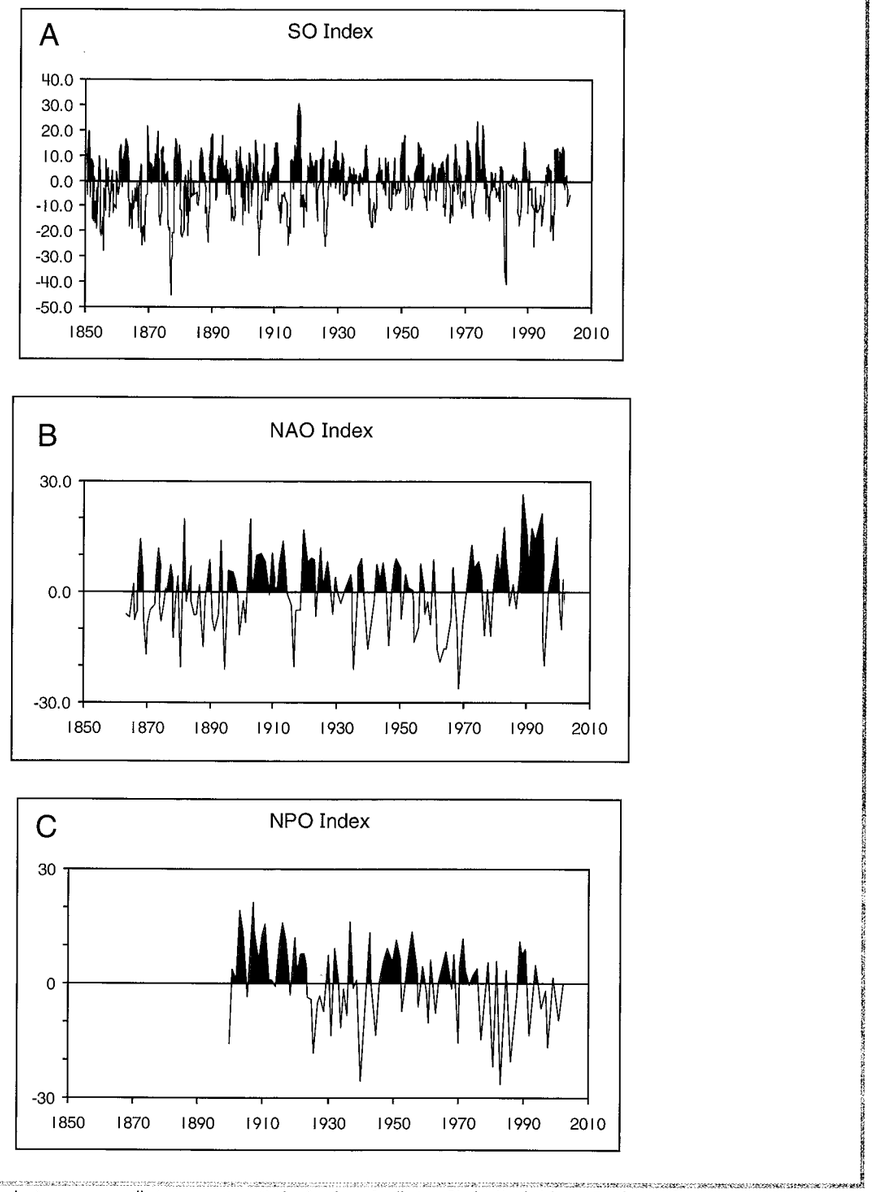

Fig. 2.8 Indices of atmospheric pressure oscillations over time A) the Southern Oscillation, B) the North Atlantic Oscillation (from Hurrell, 2002a), and C) the North Pacific Oscillation (from Hurrell, 2002b). The indices have been normalized to a mean of 0.0 hPa and a standard deviation of 10. See relevant sections in the text for further explanation.

warming is termed an El Niño event. In the early 1960s, Jacob Bjerknes recognized that warmer waters, during some El Niño events, were linked to the Southern Oscillation and the movement of warm water eastward from the west Pacific Ocean. These more widely occurring events are termed El Niño–Southern Oscillation, or for brevity, *ENSO* events. Greater amounts of warm water – along what is normally an arid coastline – lead to abnormally heavy rainfall, causing floods in the arid Andes rainfall region and drought in southern Peru, Bolivia and north-eastern Brazil. For example, in 1982–1983, in the coastal desert region of Ecuador and Peru, flash floods ripped out roads, bridges and oil pipelines. Towns were buried in mud, and shallow lakes appeared in the deserts. Irrigation-based agriculture was devastated, first by the flooding, and then by swarms of insects that proliferated under the wet conditions. The warm water also forces fish feeding on plankton to migrate to greater depths, and causes vast fish kills. Guano-producing birds feeding on anchovies die in their thousands, causing the collapse of the anchovy and fertilizer industries in Peru.

These climatic changes worldwide can be responsible for the increase of such isolated phenomena as snakebites in Montana, funnel-web spider bites in Sydney, and schizophrenia in Brazil (the latter caused by a lack of UV light due to increased cloudiness). More significantly, these changes can generate extreme economic and social repercussions, including damage to national economies, the fall of governments, and the deaths of thousands through starvation, storms and floods.

El Niño–Southern Oscillation (ENSO) events

(Philander, 1990; Glantz et al., 1991; Allan et al., 1996; Glantz, 1996; Bryant, 1997; Couper-Johnston, 2000)

Zonal, ocean–atmosphere feedback systems in the southern hemisphere are powered by three tropical heat-sources located over Africa, South America and the Indonesian–Australian maritime continent. The latter site, by far the strongest of the three systems, initiates Walker circulation. While it is relatively stable, Walker circulation is the least sedentary, because it is not anchored directly to a landmass. It is highly migratory during transition periods of the Indian monsoon, in either March–April, or August–September. Six *precursors* to the failure of Walker circulation stand out. First, sea-ice in the Antarctic and snow cover in central Asia tend to be more extensive beforehand. Second, the strength of the Indian monsoon relies heavily upon formation of an upper air, thermally driven anticyclone (between 100 and 300 hPa) over the Tibetan Plateau that leads to the formation of an easterly upper jet stream over southern India. Zonal easterly winds at 250 hPa over the Indian monsoon area also have been found to weaken up to two months before the onset of an ENSO event. Third, the Southern Oscillation appears to be a combination of the 2.2 year Quasi-Biennial Oscillation and a longer period cycle centered on a periodicity of five years. Fourth, changes in the behavior of southern hemisphere, mobile polar highs are linked to ENSO events. Strong Walker circulation is related to strong westerlies between 35° and 55°S. These westerlies appear to lock, over the Indonesian–Australian 'maritime' landmass, with heat lows developing in the austral spring. If the normally strong latitudinal flow in the mobile polar highs is replaced by *longitudinally* skewed circulation in the Australian region, then low pressure can be forced into the Pacific during the transition from northern to southern hemisphere summer. Increased southerly and south-westerly winds east of Australia preceded the 1982–1983 ENSO event, and flowed towards a South Pacific Convergence Zone that was shifted further eastwards. While highs were as intense as ever, they had a stronger meridional component, were displaced further south than normal, and were stalled over eastern Australia. Fifth, ENSO events are more likely to occur one year after the south polar vortex is skewed towards the Australian–New Zealand sector. A significant *correlation* has been found amongst this eccentricity, the Southern Oscillation, and the contemporaneous occurrence of rainfall over parts of southern hemisphere continents. Sixth, excess salinity north and south of the equator is correlated with warmer waters, presaging an ENSO event about twelve months later. The sinking of this cold salty water around the equator draws in warmer, less saline, surface water triggering the ENSO event. Finally, the causes may be interlinked. For example, more snow in Asia the winter before Walker circulation collapses may weaken the summer jet stream, leading to failure of the Indian monsoon. Alternatively, more sea-ice in the Antarctic may distort the shape and paths of mobile polar highs over the Australian continent, or displace the south polar vortex.

Whatever the cause, the movement eastward of low pressure, beyond the Australian continent, leads to westerly airflow at the western edge of the Pacific Ocean. Because there is no easterly wind holding supra-elevated water against the western boundary of the Pacific, warm water begins to move eastward along the equator (Figure 2.7b). Normally, the *thermocline* separating warm surface water from cooler water below is thicker (200 m) in the west Pacific than in the east (100 m). As warm water shifts eastward, the thermocline rises in the west Pacific. One of the first indications of an ENSO event is the appearance of colder water north of

Darwin, Australia. In the east Pacific, a layer of warm water extending 50–100 m below the ocean surface swamps cold water that is normally at the surface and maintaining the high-pressure cell off the South American coast (Figure 2.7C). As a result the thermocline deepens. As low pressure replaces high pressure over this warm water in the east Pacific, the easterlies fail altogether because there is no pressure difference across the Pacific to maintain them. Westerly winds may even begin to flow at the equator. So strong is the change that the Earth's rotation speeds up by 0.5–0.7 milliseconds as the braking effect of the easterly trades diminishes.

Cyclone development follows the location of the pool of warm water as it moves eastward towards Tahiti and Tonga. The 1982–1983 event caused widespread destruction in these areas, with Tonga receiving four tropical cyclones, each as severe as any single event in the twentieth century. The Tuamotu Archipelago, east of Tahiti, was devastated by five cyclones between January and April 1983. Not since 1906 had a cyclone occurred this far east in the tropics. In unusual circumstances, paired tropical cyclones may develop on each side of the equator in November. Because winds in tropical cyclones in each hemisphere rotate in opposite directions, coupled cyclones can combine (like an egg beater) to generate, along the equator, strong westerly wind that may accelerate water movement eastward.

At the peak of an ENSO event, a *Kelvin wave* is trapped along the east Pacific coast. Warm water and elevated sea levels spread north and south, reaching as far north as Canada. In the 1982–1983 event, temperatures were 10°C above normal and sea levels rose by 60 centimetres along the South America coastline, and by 25–30 cm along the United States west coast. The intense release of heat by moist air over the central Pacific Ocean causes the westerly jet stream in the upper atmosphere, and the position of the wintertime Aleutian Low, to shift towards the equator (Figure 2.7D). Westerly surface winds and the jet stream, rather than being deflected north around the Rocky Mountains, cross the continent at mid-latitudes. This can lead to dramatic changes in climate. For example, in the 1982–1983 ENSO event, coastal storms wreaked havoc on the luxurious homes built along the Malibu coastline of California while associated rainfall caused widespread flooding and landslides. The storms were made all the more destructive because sea levels were elevated by 25–30 cm along the entire United States west coast, from California to Washington State. Heavy snowfalls fell in the southern Rocky Mountains, record-breaking mild temperatures occurred along the American east coast and heavy rainfall fell in the southern United States.

Finally, with the spread of warm water in the northern Pacific, easterly air circulation begins to re-establish itself in the tropics. The depression of the thermocline in the east Pacific during an ENSO event causes a large wave, also called a Rossby wave, to propagate westward along the thermocline boundary. This wave is reflected off the western boundary of the Pacific and, as it returns across the Pacific, it slowly raises the thermocline to its pre-ENSO position. However, the return to Walker circulation can be anything but normal. The pool of warm water now moving back to the west Pacific drags with it exceptional atmospheric instability, and a sudden return to rainfall that breaks droughts in the western Pacific. In 1983, drought broke first in New Zealand in February, one month later in eastern Australia with rainfalls of 200–400 mm in one week, and then – over the next two to three months – in India and southern Africa.

The Southern Oscillation causes extreme, short-term climate change over 60 per cent of the globe, mainly across the southern hemisphere and certainly in North America. However, some events influence Europe. For example, the El Niño of 1997–1998 caused widespread flooding in central Europe concomitantly with flooding in central Africa, South-East Asia, and Peru. The climatic effects of an ENSO event are widespread, and its influence on both extreme climate hazards and short-term climate change is significant. Of South American countries, southern Peru, western Bolivia, Venezuela, and north-eastern Brazil are affected most by ENSO events. The 1997–1998 ENSO event destroyed $US1 billion in roads and bridges in Peru alone. The widest impact occurs over southern Africa, India, Indonesia, and Australia. For instance, in Indonesia, over 93 per cent of monsoon droughts are associated with ENSO events, and 78 per cent of ENSO events coincide with failure of the monsoon. In Australia, 68 per cent of strong or moderate ENSO events produce major droughts in the east of the continent. ENSO events have recently been shown to contribute to drought in the African Sahel region, especially in Ethiopia and Sudan.

Once an ENSO event is triggered, the cycle of climatic change operates over a minimum of two years. In historical records, the longest ENSO event lasted four years: from early 1911 to mid-1915. However, recent events have dispelled the belief that ENSO events are biennial phenomena. Following the 1982–1983 ENSO event, the warm water that traveled northward along the western coast of North America slowly crossed the north Pacific, deflecting the Kuroshio Current a decade later. As a result, northern Pacific sea surface temperatures increased abnormally, affecting general circulation across the North American continent. It is plausible that the drought on the Great Plains of the United States in the summer of 1988, and even the flooding of the Mississippi River Basin in the summer of 1993 (attributable by most to the 1990–1995 ENSO event) were prolonged North American climatic responses to the 1982–1983 El Niño. Warm water left over from the 1982–1983 ENSO event persisted in the north Pacific until the year 2000. The oceanographic effects of a major El Niño thus can have large decadal *persistence* outside the tropics.

The 1990–1995 ENSO event was even more anomalous. This event appeared to wane twice, but continued with warm central Pacific waters for five consecutive years, finally terminating in July 1995 – an unprecedented time span. Probability analysis indicates that an ENSO event of five years' duration should only recur once every 1500–3000 years. The changes in climate globally over these five years have been as dramatic as any observed in historical records. Two of the worst cyclones ever recorded in the United States, Hurricanes Andrew in Florida and Iniki in Hawaii, both in August 1992, occurred during this event. Hurricane Andrew was unusual because Atlantic hurricanes should be suppressed during ENSO events. The Mississippi River system recorded its greatest flood ever in 1993 (and then again in 1995), surpassing the flood of 1973. Record floods devastated western Europe in 1994–1995. Eastern Australia and Indonesia suffered prolonged droughts that became the longest on record. Cold temperatures afflicted eastern North America in the winter of 1993–1994, together with record snowfall, while the western half of the continent registered its highest winter temperatures ever. Record high temperatures and drought also occurred in Japan, Pakistan, and Europe in the summer of 1994.

Not all of the climatic extremes of 1990–1995 were consistent with that formulated for a composite ENSO event. For example, the Indian monsoon operated normally in 1994, while eastern Australia recorded its worst drought. Even locally within Australia, while most of the eastern half of the continent was in drought in 1992–1993, a 1000 km^2 region south of Sydney received its wettest summer on record. It is questionable whether or not all of these climatic responses can be attributed to the 1990–1995 ENSO, but they have occurred without doubt in regions where ENSO linkages or teleconnections to other climate phenomena operate. Additionally, the unprecedented nature of the 1982–1983 and 1990–1995 ENSO events may be linked to significant volcanic eruptions. While the Mexican El Chichon eruption of 1981 did not trigger the 1982–1983 El Niño, it may have exacerbated its intensity. Similarly, the 1990–1995 event corresponded well with the eruption and subsequent global cooling generated by significant volcanic eruptions in 1991 of the Philippines' Mt Pinatubo and Chile's Mt Hudson and, in 1992, of Mt Spurr in Alaska.

The events of the late twentieth century appear exceptional. They are not. Historical and proxy records are showing that mega-ENSO events occur every 400–500 years. For example, around 1100 AD, rivers in the Moche Valley of Peru reached flood levels of 18 m, destroying temples and irrigation canals built by the Chimu civilization. In the same location, the worst floods of the twentieth century (in 1926) reached depths of only 8 m. The latter event resulted in massive fires in the Rio Negro catchment of the Amazonian Basin. However, similar if not more extensive fires have occurred in 500, 1000, 1200, and 1500 AD. The 500 and 1100 AD events appear in palaeo-records from Veracruz and Mexico. In Veracruz, the latter events produced flooding and laid down sediments over a metre thick. Compared to this, the 1995 event, which has been viewed as extreme, deposited only 10–15 cm of sediment. Other mega-ENSO events occurred around 400, 1000, 1600, 2400, 4800, and 5600 BC in Veracruz. As with the prolonged 1990–1995 ENSO event, it is probable that more than one ENSO event was involved at these times. The recent prolonged 1990–1995 ENSO cycle may not be unusual, but on geological timescales represents the upper end of a shifting climate hazard regime.

La Niña events

Exceptionally 'turned on' Walker circulation is now being recognized as a phenomenon in its own right.

The cool water that develops off the South American coastline can drift northward, and flood a 1–2° band around the equator in the central Pacific with water that may be as cold as 20°C. This phenomenon is termed *La Niña* (meaning, in Spanish, 'the girl') and peaks between ENSO events. The 1988–1990 La Niña event appears to have been one of the strongest in 40 years and, because of enhanced easterly trades, brought record flooding in 1988 to the Sudan, Bangladesh and Thailand in the northern hemisphere summer. In the Sudan, the annual rainfall fell in fifteen hours, destroying 70 per cent of that country's houses. Regional flooding also occurred in Nigeria, Mozambique, South Africa, Indonesia, China, Central America, and Brazil. An unusual characteristic of this event was the late onset of flooding and heavy rain. Both the Bangladesh and the Thailand flooding occurred at the end of the monsoon season. Bangladesh was also struck by a very intense tropical cyclone in December 1988, outside the normal cyclone season.

In eastern Australia this same La Niña event produced the greatest rainfall in 25 years, with continuation of extreme rainfall events. Over 250 mm of rainfall on 30 April 1988 caused significant damage along a stretch of the coastal road between Wollongong and Sydney. Numerous landslides and washouts undermined the roadway and adjacent main railway line, leading to a total road repair cost, along a 2 kilometer stretch of coastline, of $A1.5 million (Figure 2.9). Slippage problems were still in evidence there 15 months later. The Australian summers of 1989–1990 not only witnessed record deluges but also flooding of eastern rivers on an unprecedented scale. Lake Eyre filled in both years, whereas it had filled only twice in the previous century. Towns such as Gympie, Charleville (Queensland), and Nyngan (New South Wales) were virtually erased from the map.

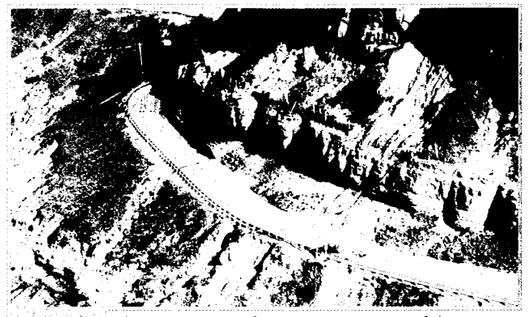

Fig. 2.9A The La Niña event of 1987–1988 was one of the strongest at the end of the twentieth century. Extreme rainfall fell throughout eastern Australia.
A) Fans deposited on the coastal road between Wollongong and Sydney following more than 250 mm of rainfall on 30 April 1988.

Fig. 2.9B B) The same rainfall event in A) caused numerous landslides and washouts that undermined the roadway and adjacent main railway. The total cost in road repairs along this 2 km stretch of coastline was $A1.5 million. Slippage problems as a result have continued for 15 years (photographs by Bob Webb, courtesy of Mal Bilaniwskyj and Charles Owen, New South Wales Department of Main Roads, Wollongong and Bellambi Offices).

Global long-term links to drought and floods

(Quinn et al., 1978; Pant & Parthasarathy, 1981; Bhalme et al., 1983; Pittock, 1984; Adamson et al., 1987)

Where the Southern Oscillation is effective in controlling climate, it is responsible for about 30 per cent of the variance in rainfall records and some of the largest death tolls in the resulting famines. Over 10 million people died in the state of Bengal during the 1769–1770 ENSO event, while the event of 1877–1878 – one of the strongest ENSO events recorded – was responsible for the deaths of 6 and 13 million people in India and China, respectively. In China people ate the edible parts of houses, while in the Sudan there were so many corpses that vultures and hyenas became fussy about the ones they would eat.

Severe droughts can occur simultaneously around the globe. In the twentieth century, the 1997–1998 ENSO event brought severe drought to South America from Colombia to north-eastern Brazil, the Caribbean, Central America, Hawaii, northern China and Korea, Vietnam, Indonesia, Papua New Guinea, and Bangladesh (East Pakistan). Southern Peru, western Bolivia, Venezuela, and north-eastern Brazil are usually affected by drought during an ENSO event; however, greatest devastation occurs in the western part of the cell in southern Africa, India, Indonesia, and Australia. There is a strong coherence in the timing of both flood and drought on the Nile in Africa, the Krishna in central India and the Darling River in Australia. As well, rainfall over parts of Australia, Argentina and Chile, New Zealand and southern Africa coincides (Figure 2.10). Most notable are the years 1894, 1910, 1917, 1961 and 1970. There is an even better correspondence between droughts in India and 'turned off' Walker circulation, or ENSO events. The severe droughts in India of 1899, 1905, 1918, 1951, 1966, and 1971 all occurred before, or at times when, El Niño events were at their peak around Christmas or when the Southern Oscillation index was negative. All of these years, except for 1951, were also times when discharges on the Nile, Krishna, and Darling River systems were either very low, or nonexistent.

A similar relationship can be traced back even further in Indonesia. This is surprising because most climatic classifications label Indonesia as a tropical country with consistent yearly rainfall. Table 2.1 summarizes the relationship between monsoon droughts and ENSO events during the period 1844–1983. In Indonesia, over 93 per cent of monsoon droughts are associated with El Niño events and 78 per cent of ENSO events coincide with failure of the monsoon. The relationships are so strong that in Java the advent of an ENSO event can be confidently used as a prognostic indicator of subsequent drought. In recent years, both India and Indonesia have established distribution infrastructures that prevent major droughts from causing starvation on as large a scale as they once did; however, the 1982–1983 event caused the Indonesian economy to stall as the country shifted foreign reserves towards the purchase of rice and wheat.

Links to other hazards

(Gray, 1984; Marko et al., 1988; Couper-Johnston, 2000)

The effect of ENSO events and the Southern Oscillation goes far beyond just drought and flood. They are responsible for the timing of many other natural hazards that can influence the heart and fabric of society. Three culturally diverse examples illustrate this

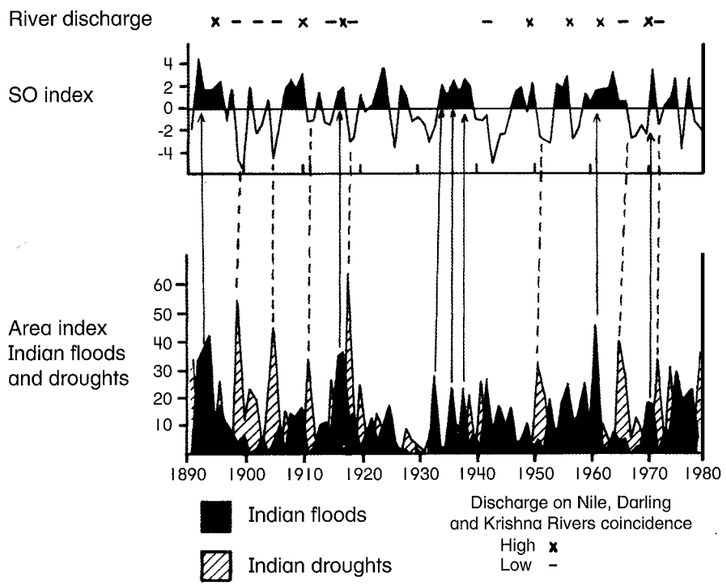

Fig. 2.10 Southern Oscillation index, drought and rainfall indices for India plus timing of coinciding low or high discharges on the Nile, Darling, and Krishna Rivers, 1890–1980 (based on Bhalme et al., 1983; Adamson et al., 1987).

Table 2.1 Comparison of drought in Indonesia with El Niño–Southern Oscillation events, 1844–1983 (Quinn et al., 1978).

1844–96		1902–83	
Drought	**El Niño event**	**Drought**	**El Niño event**
1844	1844	1902	1902
1845	1845–46	1905	1905
1850	1850	1913–14	1914
1853	none	1918–19	1918–19
1855	1855	1923	1923
1857	1857	1925–26	1925–26
1864	1864	1929	1929–30
1873	1873	1932	1932
1875	1875	1935	none
1877	1877–78	1940	1939–40
1881	1880	1941	1941
1883	none	1944	1943–44
1884–85	1884–85	1945–46	1946
1888	1887–89	1953	1953
1891	1891	no data	1954–55
1896	1896	1976	1976
		1982–83	1982

fact. First is the effect of ENSO events on civilization in Peru. The story is one of successive development and collapse of city-states. By the end of the eleventh century, most of Peru's desert coast had come under the influence of the Chimu civilization. They developed a vast network of irrigation canals stretching hundreds of kilometres between river valleys. Around 1100 AD, extraordinary flooding exceeding 18 m depths wiped out all of their engineering achievements in the Moche Valley. Rival city-states were also affected; however the Chimu undertook military action to expand their area of influence so that they could relocate. While the rival states sank into revolt and anarchy, the Chimu conquests succeeded to rival the Incas in power. This example was but one phase in a sequence of rapid cultural advancement, abandonment, and expansion of opportunistic city-states triggered by ENSO events along the west coast of South America. Over four centuries, this process has covered an area of 30 000 km^2 of coastal plain.

The second example is the historical development of Ethiopia. The ENSO events of 1888 and 1891 killed a third of this country's population at a time when the Italians hoped to establish a colonial empire in the Horn of Africa. Other European countries – mainly the British – had taken advantage of ENSO-related droughts to expand their empires in Africa. However, Emperor Menilek took advantage of his weakened enemies to consolidate his position as the country's absolute ruler. When the La Niña of 1892 brought rain and harvests to feed his army, Menilek was able to defeat the Italians at the Battle of Adowa and become the first African ruler to repel colonialism in Africa.

Third is the effect of the 1982–1983 ENSO event on Australia. This brought the worst drought Australia has experienced. Approximately $A2000 million was erased from the rural economic sector as sheep and cattle stocks were decimated by the extreme aridity. Wheat harvests in New South Wales and Victoria were, respectively, 29 per cent and 16 per cent of the average for the previous five years. The resulting lack of capital expenditure in the rural sector deepened what was already a severe recession, and drove farm machinery companies such as International Harvester and Massey Ferguson into near bankruptcy. By January 1983, dust storms in Victoria and New South Wales had blown away thousands of tons of topsoil. Finally, in the last stroke, the Ash Wednesday bushfires of 16 February 1983, now viewed as one of the greatest natural *conflagrations* observed by humans, destroyed another $A1000 million worth of property in South Australia and Victoria. At the peak of the event, Malcolm Fraser's Liberal–National Party coalition government called a national election. The timing could not have been worse, and the government of the day was swept convincingly from power.

Other natural hazards are associated with the Southern Oscillation. This is exemplified in Figure 2.11 for Australia between 1851 and 1980. (The index here is part of the one used in Figure 2.8.) Shaded along this index are the times when eastern Australia was either in drought or experiencing abnormal rainfall. Sixty-eight per cent of the strong or moderate ENSO events between 1851 and 1974 produced major droughts in eastern Australia. Sixty per cent of all recoveries after an ENSO occurrence led to abnormal rainfall and floods. Figure 2.11 also includes the number of tropical cyclones in the Australian region between 1910 and 1980; the discharge into the Murray River of Victoria's central north Campaspe River between 1887 and 1964; beach change at Stanwell Park, south of Sydney, between 1930 and 1980, described in Chapter 8; rainfall this century at Helensburgh, south of Sydney; and the

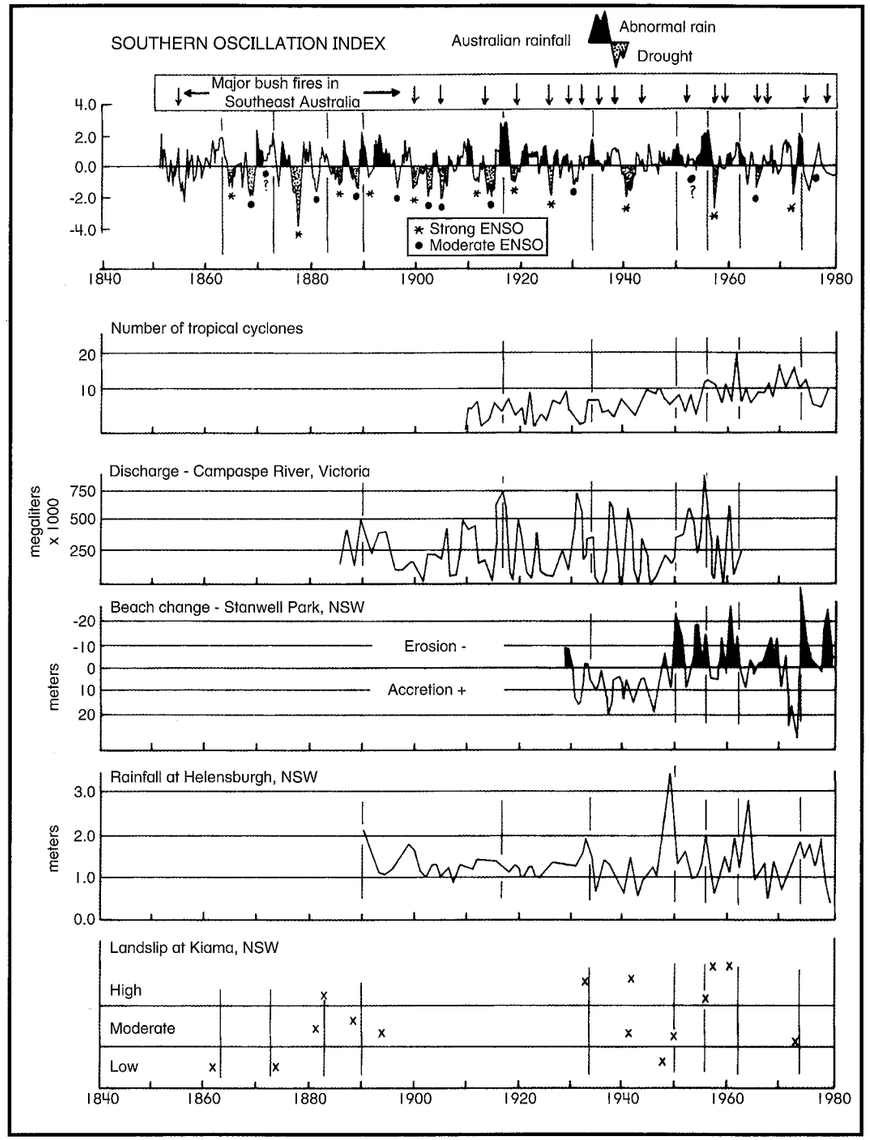

Fig. 2.11 Time series of the Southern Oscillation index, major bushfires (from Luke & McArthur, 1978), Australian cyclone frequency (from Lourensz, 1981), Campaspe River discharge (from Reichl, 1976), beach change at Stanwell Park (from Bryant, 1985), rainfall near Sydney, and landslip incidence at Kiama (courtesy Jane Cook, School of Education, University of Wollongong).

incidence of landslip in the Kiama area, south of Sydney, between 1864 and 1978. Drawn on the diagram are lines passing through all data at the times when the Southern Oscillation was strongly 'turned on'. At this time, tropical cyclones were more frequent, the Campaspe River discharge high, Sydney rainfall heavy, beach erosion at Stanwell Park more severe, and Kiama landslip more frequent. The diagram indicates that 'turned on' Walker circulation results in this predictable geomorphic response. The 1933, 1951 and 1961 periods of strong

Walker circulation show up in all five time series at both regional and localized levels. The reverse conditions apply during ENSO events, except for the frequency of tropical cyclones in the Australian region; historically this is not well correlated to ENSO events. This is owing to the fact that many cyclones are still counted within the Australian region even though they have shifted eastward during these events. More importantly, the Southern Oscillation appears to switch months in advance of the arrival of the meteorological conditions driving these responses. For instance, the heavy rainfall in eastern Australia, beginning in the autumn of 1987, was predicted 12 months in advance. Unfortunately, while the timing of rain can be forecast, its precise location or the amounts that may fall remain unpredictable because of the spatial variability of precipitation along the coast. Even during the worst of droughts, some areas of eastern Australia received normal rainfall.

Links to other hazards are also appearing globally as researchers rapidly investigate teleconnections between hazards and the Southern Oscillation. For example, droughts are often followed by extensive fires in Florida, eastern Russia, and Indonesia. There is also heavier precipitation, mainly falling as snow in north-eastern United States and south-eastern Canada. The 1997–1998 ENSO event produced five days of *freezing rain* in this region that downed 120 000 km of power and telephone lines, paralyzing the city of Montreal. The duration and incidence of tropical cyclones in the equatorial Atlantic is profoundly depressed during ENSO years (Figure 2.12). Here, upper tropospheric winds between 0° and 15°N must be easterly, while those between 20° and 30°N must be westerly, before easterly wave depressions and disturbances develop into tropical cyclones (hurricanes). During ENSO events, upper westerlies tend to dominate over the Caribbean and the western tropical Atlantic, giving conditions that suppress cyclone formation. Years leading up to an ENSO event have tended to produce the lowest number of tropical cyclone days in the Atlantic over the past century. Additionally, since 1955, the number of icebergs passing south of 48°N has been highly correlated to the occurrence of ENSO events. ENSO events occur concomitantly with a strengthened Icelandic Low that results in stronger winds along the North American east coast. This exacerbates the production and southward movement of icebergs. Both the 1972–1973 and 1982–1983 ENSO events produced over 1500 icebergs south of 48°N, a number that dramatically contrasts with non-ENSO years when fewer than one hundred icebergs per year were recorded this far south. Early detection of the onset of ENSO events can thus provide advance warning not only of drought and rainfall over a significantly large part of the globe, but also of the occurrence of numerous other associated hazards.

Other Oscillation phenomena

(Trenberth & Hurrell, 1994; Hurrell, 1995; Villwock, 1998; Stephenson, 1999; Boberg & Lundstedt, 2002; Hurrell et al., 2002)

North Atlantic Oscillation

There are two other regions: the north Atlantic and Pacific Oceans where pressure oscillates on the same scale as the Southern Oscillation. Variations in the intensity of atmospheric circulation at these locations are known as *North Atlantic Oscillation* (NAO) and the *North Pacific Oscillation* (NPO). Whereas the Southern Oscillation characterizes zonal pressure fluctuations in the tropics across the Pacific, the NAO and NPO are meridional air circulation phenomena reflecting inter-annual variability in the strength of Rossby waves in the northern hemisphere. The North Atlantic Oscillation also reflects major temperature differences in winter. An index of the NAO since 1864 has been constructed using the normalized atmospheric pressure between the Icelandic Low, measured at Stykkisholmur/Reykjavik, Iceland, and the Azores High, measured at Lisbon (Figure 2.8). Positive values of the index indicate stronger-than-average westerlies. Air temperature fluctuations are best characterized by the winter temperature between Jakobshavn, West Greenland, and Oslo, Norway. Significant environmental changes throughout the twentieth century have been associated with the NAO. These include variations in wind strength and direction, ocean circulation, sea surface temperatures, precipitation, sea-ice extent, and changes in marine and freshwater ecosystems. The North Atlantic Oscillation influences an area from Siberia to the eastern seaboard of the United States. Given the magnitude and extent of the NAO, it is surprising that little attention was given to it until the 1990s.

The NAO undergoes large variation from year to year and, more importantly, at decadal time scales. However, large changes can also occur during a winter season. Hence it is difficult to characterize northern hemisphere winters as completely severe or benign. This probably reflects the fact that climate processes are random over time. Large amplitude anomalies in wintertime stratospheric winds precede anomalous behavior of the NAO by one to two weeks. Changes to the strength and pathway of mobile polar highs and the amplitude of Rossby waves in the polar jet stream also correspond to winter anomalies. Similar to the Southern Oscillation, short-term alterations are also preceded by changes in sea surface temperature about nine months in advance. Together the NAO and SO account for 50 per cent (34 per cent and 16 per cent, respectively) of the variation in winter temperatures in the northern hemisphere outside the tropics. However, the Southern and North Atlantic Oscillations act independently of each other. The eastern United States and adjacent Atlantic region are the only areas where both phenomena always act together.

There are two distinct decadal phases associated with the NAO. When the index is positive, atmospheric pressure is low around Iceland and high in the Azores. Sea surface temperatures off the United States eastern seaboard and western Europe are warmer than normal, while those in the western north Atlantic are cooler than average (Figure 2.13a). These aspects enhance meridional air circulation in the atmosphere, strengthening westerly winds at temperate latitudes and forcing warm, moist air from the Atlantic Ocean over northern Europe. Hence land temperatures are warmer adjacent to these pools of warmer ocean waters, leading to milder winters. Temperatures are cool over North Africa, the Middle East, eastern Canada, and Greenland. The flux of heat across the north Atlantic produces more intense and frequent storms, a fact that has been more obvious since 1970 (Figure 2.14). As a result, wave heights increase in the north-east Atlantic and decrease south of 40°N latitude. This is paralleled by changes in precipitation – wetter over Scandinavia and drier in the Mediterranean. Over northern Africa, more dust moves from the Sahara into the Atlantic Ocean. Sea-ice also extends further south over the west Atlantic, while retreating east of Greenland. These effects are either wind- or temperature-driven. In the negative phase, the pressure gradient between Iceland and the Azores is weakened, the Mediterranean region is wetter and warmer, and northern Europe is cooler and drier (Figure 2.13b). While storms off the east coast of the United States may be more frequent, they are virtually absent off western Europe. These periods of anomalous circulation patterns have persisted over long periods. For example, the NAO index was positive from the turn of the twentieth century until about the 1930s. During the 1960s, the NAO index was negative with severe winters across northern Europe. Since the early 1970s, circulation has been locked into a positive phase with warmer temperatures than average over Europe and cooler ones over eastern Canada and Greenland.

North Pacific Oscillation

The North Pacific Oscillation (NPO) measures the strength and position of the Aleutian low-pressure system, mainly in winter. Because there are few recording stations in the north Pacific, an index

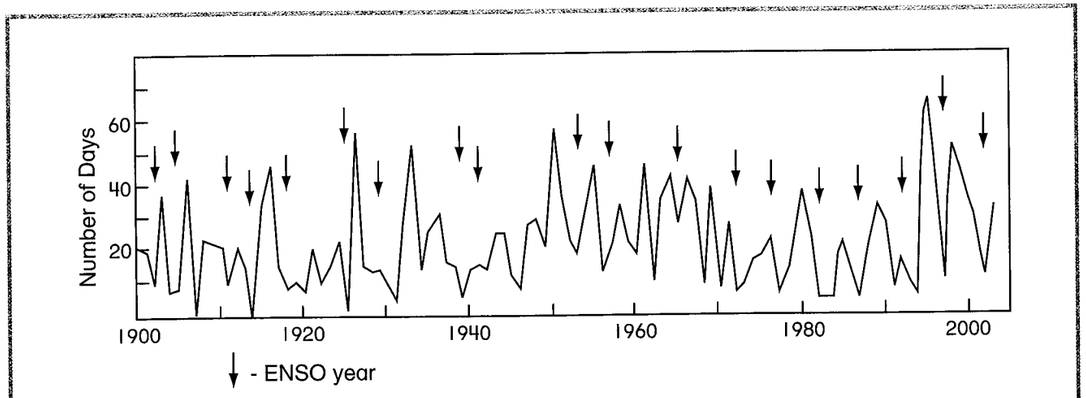

Figure 2.12 Number of hurricane days in the North Atlantic–Caribbean Sea region, 1900–2003 (based on Gray, 1984; Hurricane Research Division, 2003).

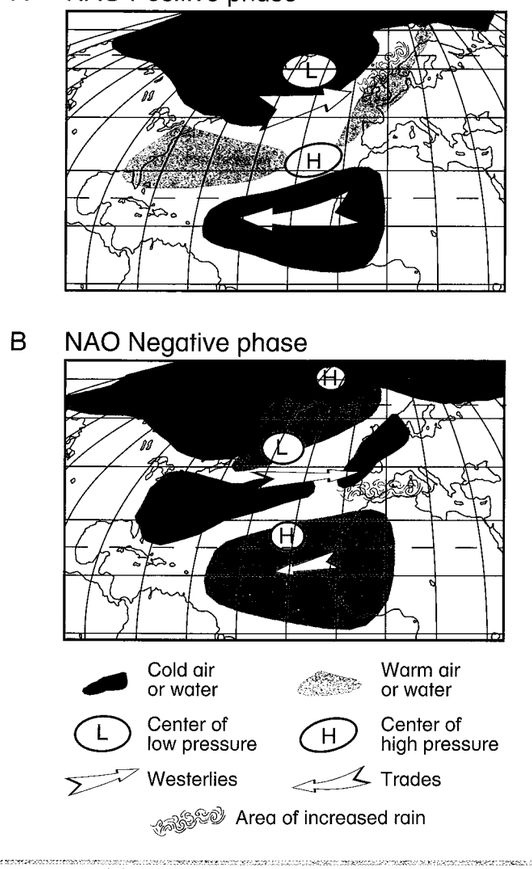

Fig. 2.13 Atmospheric circulation patterns and climatic impacts associated with A) positive and B) negative phases of the North Atlantic Oscillation (based on Stephenson, 1999).

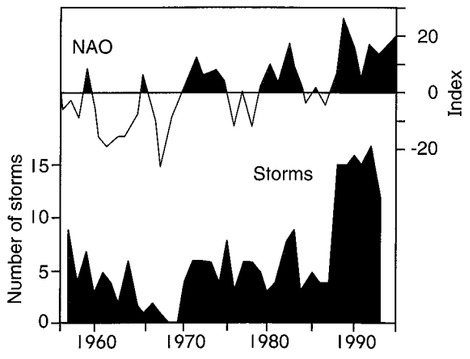

The number of winter storms in the north Atlantic between 1956 and 1994 with pressure below 950 hPa (Villwock, 1998).

characterizing this oscillation has been built using average surface air pressure over the region 30°N–65°N, 160°E–140°W (Figure 2.8). Over the north Pacific Ocean, atmospheric pressure near the Aleutian Islands varies out-of-phase with that to the south, seesawing around the mean position of the Pacific subtropical jet stream. Over North America, variations in atmospheric pressure over western Canada and the north-western United States are negatively correlated with those over the south-eastern United States; but positively correlated with the subtropical Pacific. Changes in these centers occur concomitantly with changes in the amplitude of Rossby waves and the intensity of mobile polar highs. The NPO is linked to changes in tropical Pacific sea surface temperatures associated with the ENSO phenomenon.

In this respect, the NPO is probably the temperate north Pacific extension of the Southern Oscillation, with sea surface temperature changes in the north Pacific lagging those in the tropics by three months. However, the NPO does have its own independent features. Of all atmospheric indices, the North Pacific Oscillation shows the greatest well-defined trend over time (Figure 2.8). The index has been steadily declining, although there is significant year-to-year variation. Concomitantly with this trend, the Aleutian Low has intensified and shifted eastward in winter. As a result, storm tracks have shifted southward. This has resulted in warmer and moister air being transported northward along the west coast of North America into Alaska. Sea surface temperatures in the north Pacific have cooled, but sea-ice has decreased in the Bering Sea.

ASTRONOMICAL CYCLES

Solar cycles

(Shove, 1987; Hoyt & Schatten, 1997; Boberg & Lundstedt, 2002)

Sunspots are surface regions of intense disturbance of the sun's magnetic field: 100–1000 times the sun's average. The spots themselves appear dark, because the magnetic field is so strong that convection is inhibited and the spot cools by radiation emission. However, the total amount of radiation given out by the sun increases towards peaks in sunspot activity. The sun has a 22-year magnetic cycle, consisting of two 11-year sunspot cycles. In Figure 2.15, these are plotted back to 1500 AD. The 22-year periodicity known as the *Hale Cycle* is evident as an enhanced peak in sunspot numbers in this figure. There are also other periodicities, at 80–90 years and 180 years, in the number of sunspots. The interaction of these cycles has produced periods where there was little sunspot activity. Two of these, the Maunder and Dalton Minimums, in the late seventeenth and early nineteenth centuries, respectively, are evident in Figure 2.15. Both are correlated to periods of cooler climate, at least in the northern hemisphere. The *Maunder Minimum* is also known as the *Little Ice Age*. Periods of high activity correlate with warmer climate. This occurred in the thirteenth century during the Medieval Maximum and over the last 150 years concurrent with modern global warming.

Other phenomena characterize our sun. *Solar flares* – representing ejection of predominantly ionized hydrogen in the sun's atmosphere at speeds in excess of 1500 km s^{-1} – develop in sunspot regions. Flares enhance the solar wind that ordinarily consists of electrically neutral, ionized hydrogen. Accompanying any solar flare is a pulse of electro-magnetic radiation that takes eight minutes to reach the Earth. This radiation, in the form of soft X-rays (0.2–1.0 nm wavelengths), interacts with the Earth's magnetic field, increasing ionization in the lowest layer of the ionosphere at altitudes of 65 km. The enhanced solar wind arrives one to two days after this magnetic pulse and distorts the magnetosphere, resulting in large, irregular, rapid worldwide disturbances in the Earth's geomagnetic field. Enhanced magnetic and ionic currents during these periods heat and expand the upper atmosphere. The solar wind also modulates cosmic rays affecting the Earth. When the solar wind is strong, cosmic rays are weak – resulting in decreased cloud formation and warmer surface air temperatures. Cloud cover decreases around 3–4 per cent between troughs and peaks in *geomagnetic activity*. Solar flare activity and the strength of the solar wind are weakly correlated to the number of sunspots (Figure 2.15b). Thus, geomagnetic activity is a better indicator of solar influence on climate than the number of sunspots. While solar activity on a timescale of weeks can affect the temperature structure of the stratosphere, there is no proven mechanism linking it to climatic change over longer periods near the surface of the Earth. This fact has tended to weaken the scientific credibility of research into the climatic effects of solar cycles.

Despite this, the literature is replete with examples showing a correlation between climate phenomena and solar activity in the form of sunspots. Much of the emphasis has been upon a solar sunspot–global temperature association. High sunspot activity leads to warmer temperatures and more precipitation, although this relationship is consistent neither over time nor the surface of the globe. This discussion is beyond the scope of this text and the curious reader should see Hoyt and Schatten (1997) for further information. More substantial is the fact that thunderstorm, lightning and tropical cyclone activity worldwide increases during periods of sunspot activity. In addition, 15 per cent of the variation in the position of storm tracks in the north Atlantic and Baltic Sea can be

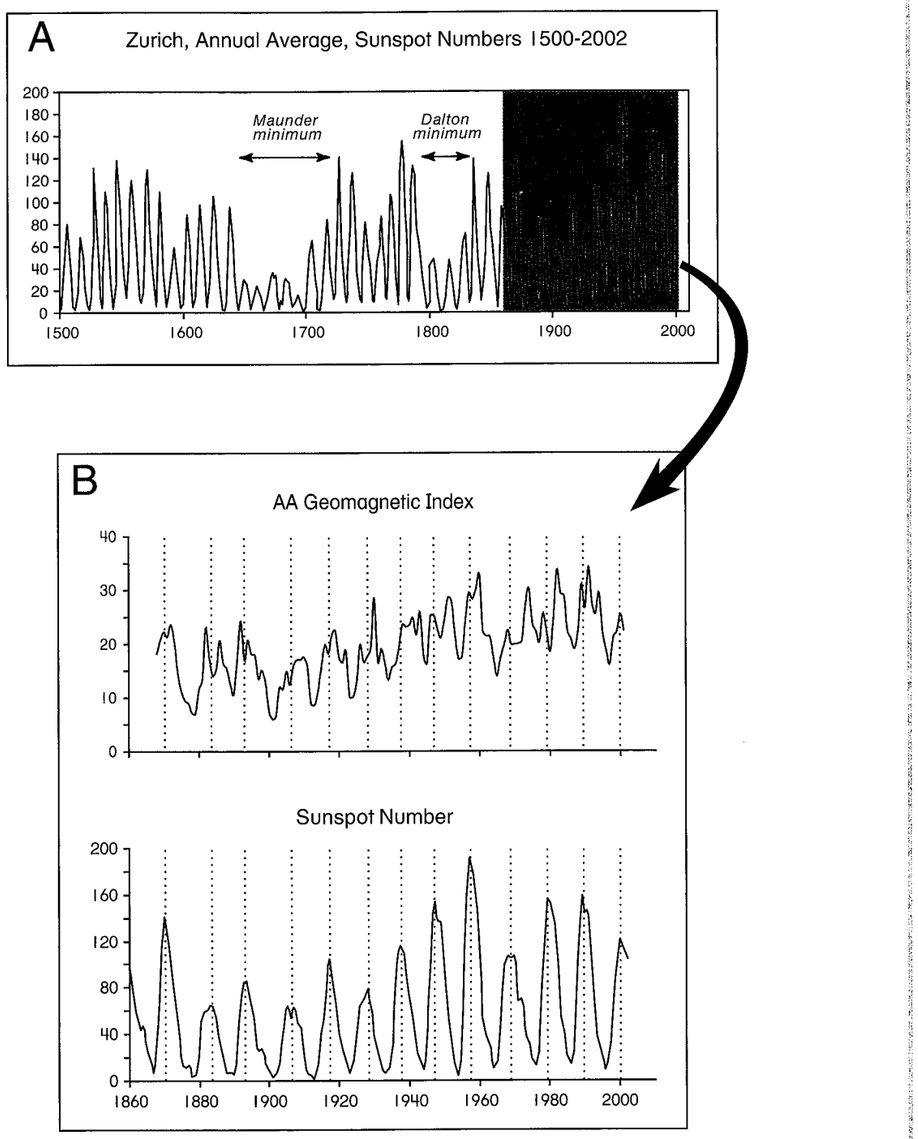

Fig. 2.15 A) Time series of the annual average, Zurich sunspot number between the years 1500 and 2002. Values between 1500 and 1749 are from Shove (1987), between 1750 and 2002 from the National Geophysical Data Centre (2003a). B) Detail of the Zurich sunspot record between 1860 and 2002 with the annual AA geomagnetic index superimposed. Latter from National Geophysical Data Centre (2003b).

accounted for by solar variations. Storm tracks shift southward by 3–4° latitude in both regions when sunspot activity is highest. Forest fires are more numerous in North America at peaks in the sunspot cycle. The decadal variance in the North Atlantic Oscillation is also positively correlated to enhanced geomagnetic activity. Finally, there are solar periodicities in the frequency of earthquakes and volcanic eruptions. The reason for the latter is beyond the scope of this text.

The 18.6-year M_N lunar cycle

(Tyson et al., 1975; Currie, 1981, 1984; Wang & Zhao, 1981)

The 18.6-year lunar tidal cycle (M_N) represents a fluctuation in the orbit of the moon. The moon's axis of orbit forms a 5° angle with the sun's equator as shown in Figure 2.16; however, with each orbit the moon does not return to the same location relative to the sun. Instead, it moves a bit further in its orbit. The process is analogous to a plate spinning on a table. The plate may always be spinning at the same angle relative to the table, but the high point of the plate does not occur at the same point. Instead, it moves around in the direction of the spin. The moon's orbit does the same thing, such that 9.3 years later the high point of the orbit is at the opposite end of the solar equator, and 9.3 years after that it returns to its original position. Thus, there is an 18.6-year perturbation in the orbit of the moon. This perturbation appears trivial until you consider the moon's orbit in relation to the Earth (Figure 2.17). Relative to the Earth, the solar equator moves seasonally, reaching a maximum of 23.46°N of the equator on 22 June and a minimum of 23.46°S of the Earth's equator on 22 December. If the moon–sun orbital configuration in Figure 2.16a is superimposed onto the Earth, then the moon is displaced in its orbit closest to the Earth's poles, 28.5° (23.5° + 5°) north and south of the equator. The moon's gravitational attraction on the Earth is slightly greater when the moon is displaced poleward. In 9.3 years' time, the moon will move to the opposite side of the sun's equator. Relative to the Earth, the moon will be closer to the equator, or in its minimum position (Figure 2.17b). Although it is only 3.7 per cent the daily effect, the gravitational effect of the M_N tide has two to three years to act on any standing, planetary wave phenomena.

Standing atmospheric waves, such as Rossby waves embedded in the jet stream (Figure 2.4), are amplified by the M_N lunar tide. An 18–20 year periodicity appears in sea level, air pressure, and temperature records at locations beneath the jet stream from Japan to Scandinavia. Detailed examination of the occurrence of drought on the United States Great Plains since 1800 shows a strong link between drought and the 18.6-year M_N lunar cycle. A 20-year cycle is also evident in rainfall over the Yangtze River Basin of China, coinciding with the American pattern and the Indian flood record. In the southern hemisphere, a 20-year periodicity appears in summer rainfall in

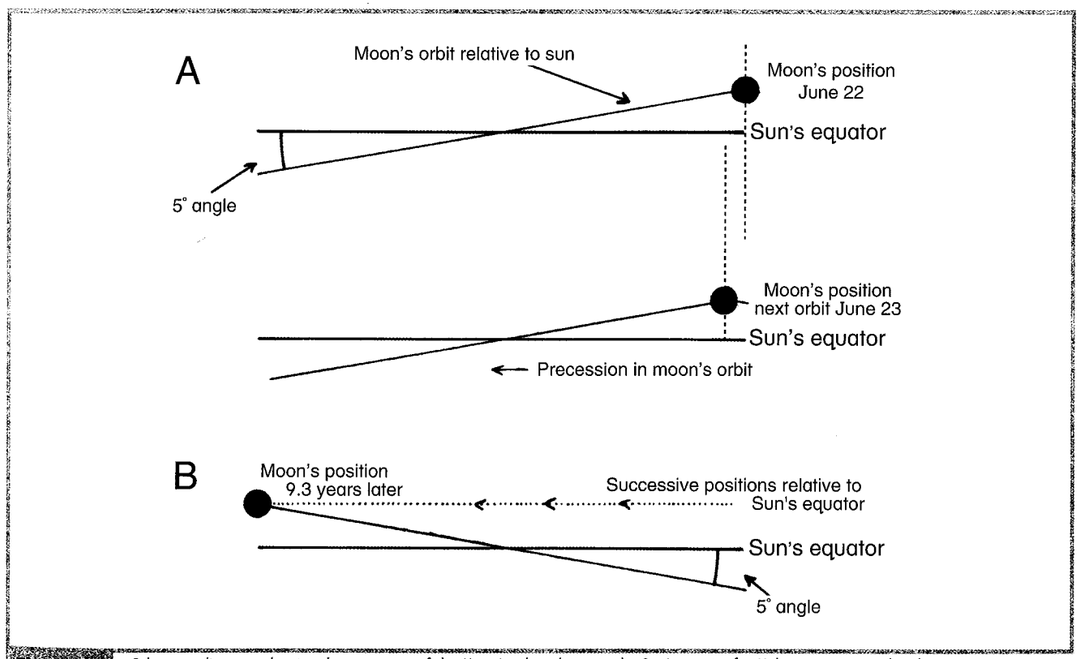

Fig. 2.16 Schematic diagrams showing the precession of the Moon's orbit relative to the Sun's equator for A) lunar maxima and B) lunar minima.

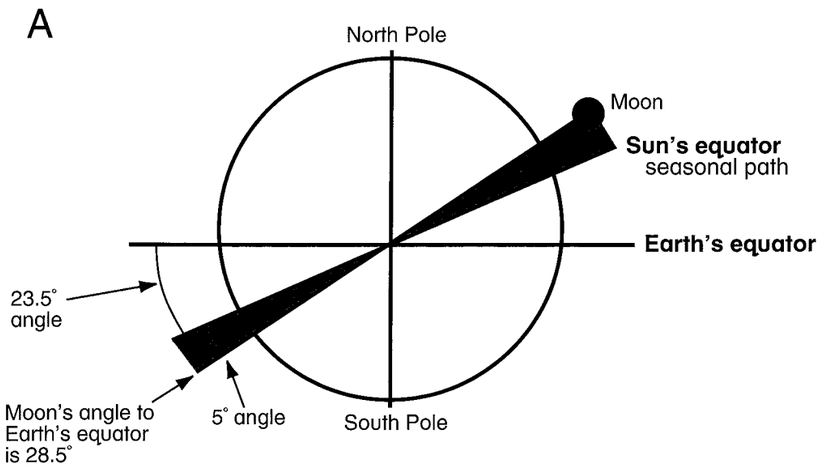

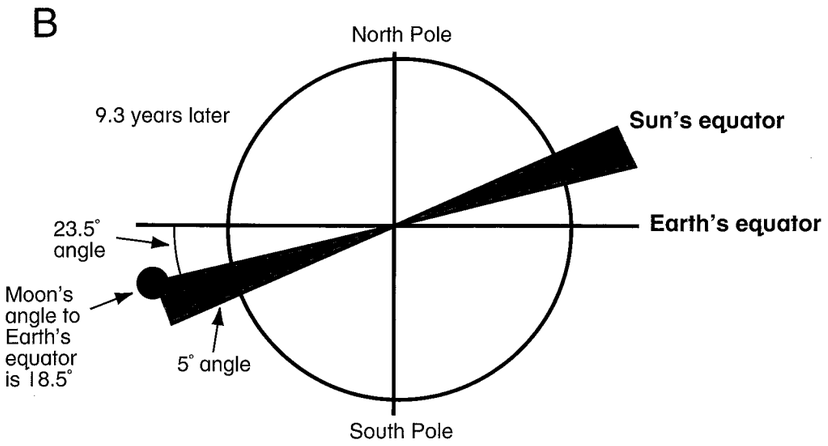

Fig. 2.17 Schematic presentations of the 18.6-year lunar orbit relative to the Earth for A) lunar maxima and B) lunar minima.

southern Africa and eastern Australia. A sampling of these associations worldwide is presented for the western United States and Canada, northern China, India, the Nile region of Africa, and the mid-latitudes of South America (Table 2.2). In all cases, except for India, the mean discrepancy between the occurrence of the hazard and peaks in the lunar tide is less than one year. Not only is the 18.6-year cycle dominant, but the data also show temporal and spatial *bistable phasing*. In this process, drought may coincide with maxima in the 18.6-year lunar cycle for one period, but then suddenly switch to a minimum. This 'flip-flop' happens every 100–300 years, with the most recent occurring at the turn of the twentieth century in South America, China, Africa, and India. On the Great Plains, no bistable 'flip-flop' has occurred since 1657; however, the last lunar cycle maximum in 1991 witnessed flooding instead of drought in this region. At present, disparate regions of the globe's major wheat growing areas undergo synchronous periods of drought that have major implications for the price of grain and the relief of famine-stricken regions.

Table 2.2 Timing of flood (F) and drought (D) in North America, northern China, Patagonia, the Nile valley, India and the coincidence with the 18.6 year lunar tide

Lunar Maxima	Canadian Prairies	United States Great Plains	N. China	Patagonian Andes	Nile in Africa	India
1583	1581D		1582D			
1601	1601D		1600D	1606F		
1620	1622D		1620D	1621F		
1638	1640D		1640D	1637F		
1657	1652F		1659D	1656F		
1676	1674F		1678D	1675F		
1694	1694F			1693F		
1713	1712F			1710F	1713D	
1731	1729F			1727F	1733D	
1750	1752F			1752D	1750D	
1768	1768F			1768D	1766D	
1787	1786F			1784D	1789D	
1806	1805F	1805D	1806F	1802D	1806D	
1824	1823F	1824D	1823F	1822D	1822D	
1843	1843F	1844D	1846D	1841D	1837D	
1861	1859F	1861D	1862D	1864D		
1880	1881F	1879D	1881D	1880D	1885D	
1899	1900F	1901D	1900D	1895D	1902D	1902D
1918	1916F	1919D	1918D	1918F	1917F	1913F
1936	1932F	1935D	1935F	1937F	1936F	1939F
1955	1953F	1955D	1954F	1956F	1953F	1958F
1973	1975F	1975D	1974F	1973F	1975F	1976F
1991	1995F	1993F	1990F	1992F	1996F	1990F

Sources: Currie (1984) and various internet searches. Since 1980, plotted rainfall anomalies for each region using http://climexp.knmi.nl/fieldplot.cgi?someone@somewhere+gpcp

CONCLUDING COMMENTS

The dominant factor controlling air movement across the surface of the Earth is the movement of cold polar air in the form of mobile polar highs from the poles towards the equator. This drives global air circulation and satisfies the requirement in the atmosphere to balance the inequality in heating and cooling between the equator and poles, respectively. The concept of mobile polar highs implies that the climate of high latitudes is the key to world climate and global climate change. Superimposed upon this meridional exchange are zonal processes controlled by ocean–atmosphere interactions. Chief amongst these is the Southern Oscillation. While droughts and floods have plagued people throughout recorded history, and are probably responsible for the greatest loss of life of any natural hazards, the realization is that they represent inseparable hazards that follow each other in time as night does day. Not only are the two events linked, but their occurrence is also remarkably coincident across the globe. They are intricately connected to the Southern Oscillation and other spatial cyclic phenomena such as the North Atlantic and North Pacific Oscillations. Other hazards – such as tropical and extra-tropical cyclones, wave erosion, and land instability – are also correlated to the Southern Oscillation, and thus subject to prediction. At mid-latitudes in the northern hemisphere, storminess is more important. Here, the North Atlantic Oscillation is the controlling factor. Similar influences may occur in western North America due to changes in sea surface temperature in the north Pacific.

There is now indisputable proof that droughts and subsequent heavy rainfall periods are cyclic, not only in semi-arid parts of the globe, but also in the temperate latitudes. This cyclicity correlates well with the 18.6-year lunar tide in such diverse regions as North America, Argentina, northern China, the Nile Valley, and India. There is also evidence that the 11-year sunspot cycle is present in rainfall time series in some countries. Long-term astronomical periodicities, especially in the northern hemisphere, permit scientists to pinpoint the most likely year that drought or abnormal rainfall will occur, while the onset of an ENSO event with its global consequences permits us to predict climatic sequences up to nine months in advance. These two prognostic indicators should give countries time to modify both long- and short-term economic strategies to negate the effects of drought or heavy rainfall.

Unfortunately, very few governments in the twentieth century have lasted longer than 11 years – the length of the shortest astronomical cycle. Realistically, positive political responses – even in the United States – to dire drought warnings are probably impossible. Societies must rely upon the efficiency and power of their permanent civil services to broadcast the warnings, to prepare the programs reducing the effects of the hazards, and to pressure governments of the day to make adequate preparations.

Finally, it should be realized that the astronomical cycles and oscillations such as the Southern or North Atlantic Oscillations account for only 15–30 per cent of the variance in rainfall in countries where their effects have been defined. This means that 70 per cent or more of the variance in rainfall records must be due to other climatic factors. For example, during the drought that affected eastern Australia in 1986–1987, Sydney was inundated with over 400 mm of rainfall, breaking the previous 48-hour rainfall record, and generating the largest storm waves to affect the coast in eight years. This randomness exemplifies the importance of understanding regional and local climatic processes giving rise to climatic hazards. These regional and local aspects will be described in the following chapters.

REFERENCES AND FURTHER READING

Adamson, D., Williams, M.A.J. and Baxter, J.T. 1987. Complex late Quaternary alluvial history in the Nile, Murray–Darling, and Ganges Basins: three river systems presently linked to the Southern Oscillation. In Gardiner, V. (ed.) *International Geomorphology* Pt II, Wiley, NY, pp. 875–887.

Allan, R., Lindesay, J. and Parker, D. 1996. *El Niño Southern Oscillation and Climatic Variability*. CSIRO Publishing, Melbourne.

Bhalme, H.N., Mooley, D.A. and Jadhav, S.K. 1983. Fluctuations in the drought/flood area over India and relationships with the Southern Oscillation. *Monthly Weather Review* 111: 86–94.

Boberg, F. and Lundstedt, H. 2002. Solar wind variations related to fluctuations of the North Atlantic oscillation. *Geophysical Research Letter* 29(15) 10.1029/2002GL014903.

Bryant, E.A. 1985. Rainfall and beach erosion relationships, Stanwell Park, Australia, 1895–1980: worldwide implications for coastal erosion. *Zeitschrift für Geomorphologie Supplementband* 57: 51–66.

Bryant, E.A. 1997. *Climate Process and Change*. Cambridge University Press, Cambridge.

Bryson, R. and Murray, T. 1977. *Climates of Hunger*. Australian National University Press, Canberra.

Couper-Johnston, R. 2000. *El Nino: The Weather Phenomenon That Changed the World*. Hodder and Stoughton, London.

Currie, R.G. 1981. Evidence of 18.6 year M_N signal in temperature and drought conditions in N. America since 1800 A.D. *Journal Geophysical Research* 86: 11055–11064.

Currie, R.G. 1984. Periodic (18.6-year) and cyclic (11-year) induced drought and flood in western North America. *Journal Geophysical Research* 89(D5): 7215–7230.

Glantz, M.H. 1996. *Currents of Change: El Niño's Impact on Climate and Society*. Cambridge University Press, Cambridge.

Glantz, M.H., Katz, R.W. and Nicholls, N. 1991. *Teleconnections Linking Worldwide Climate Anomalies: Scientific Basis and Societal Impact*. Cambridge University Press, Cambridge.

Gray, W.M. 1984. Atlantic seasonal hurricane frequency Part I: El Niño and 30 mb quasibiennial oscillation influences. *Monthly Weather Review* 112: 1649–1667.

Hoyt, D.V. and Schatten, K.H. 1997. *The Role of the Sun in Climate Change*. Oxford University Press, Oxford.

Hurrell, J.W. 1995. Decadal trends in the North Atlantic Oscillation: Regional temperatures and precipitation. *Science* 269: 676–679.

Hurrell, J.W. 2002a. *North Atlantic Oscillation (NAO) indices information: Winter (Dec–Mar)*. <http://www.cgd.ucar.edu/~jhurrell/nao.stat.winter.html>

Hurrell, J.W. 2002b. *North Pacific (NP) index information*. <http://www.cgd.ucar.edu/~jhurrell/np.html>

Hurrell, J.W., Kushnir, Y., Ottersen, G. and Visbeck, M. (eds) 2002. *The North Atlantic Oscillation: Climatic Significance and Environmental Impact*. American Geophysical Union, Washington.

Hurricane Research Division 2003. *What are the most and least tropical cyclones occurring in the Atlantic basin and striking the USA?*. United States Department of Commerce. <http://www.aoml.noaa.gov/hrd/tcfaq/tcfaqE.html>

Jet Propulsion Laboratory 1995a. *TOPEX/POSEDON: Wind Speed, January*. <http://education.gsfc.nasa.gov/experimental/all98invProject.Site/Pages/trl/inv4-7WIND_SPEED_JAN.html>

Jet Propulsion Laboratory 1995b. *TOPEX/POSEDON: Wind Speed, July*. <http://education.gsfc.nasa.gov/experimental/all98invProject.Site/Pages/trl/inv4-7WIND_SPEED_JUL.html>

Lamb, H.H. 1982. *Climate, History and the Modern World*. Methuen, London.

Lamb, H.H. 1986. The causes of drought with particular reference to the Sahel. *Progress in Physical Geography* 10(1): 111–119.

Leroux, M. 1993. The Mobile Polar High: a new concept explaining present mechanisms of meridional air-mass and *energy* exchanges and global propagation of palaeoclimatic changes. *Global and Planetary Change* 7: 69–93.

Leroux, M. 1998. *Dynamic Analysis of Weather and Climate: Atmospheric Circulation, Perturbations, Climatic Evolution*. Wiley-Praxis, Chichester.

Lourensz, R.S. 1981. *Tropical Cyclones in the Australian Region July 1909 to June 1980*. Australian Bureau of Meteorology, Australian Government Publishing Service, Canberra.

Luke, R.H. and McArthur, A.G. 1978. *Bushfires in Australia*. Australian Government Publishing Service, Canberra.

Marko, J.R., Fissel, D.B. and Miller, J.D. 1988. Iceberg movement prediction off the Canadian east coast. In El-Sabh, M.I. and Murty, T.S. (eds) *Natural and Man-made Hazards*. Reidel, Dordrecht, pp. 435–462.

National Geophysical Data Center 2003a. *Sunspot numbers*. <ftp://ftp.ngdc.noaa.gov/STP/SOLAR_DATA/SUNSPOT_NUMBERS>

National Geophysical Data Center 2003b. *AA Index*. <ftp://ftp.ngdc.noaa.gov/STP/SOLAR_DATA/RELATED_INDICES/AA_INDEX/>

Pant, G.B. and Parthasarathy, B. 1981. Some aspects of an association between the Southern Oscillation and Indian summer monsoon. *Archiv für Meteorologie, Geophysik und Bioklimatologie*. B29: 245–252.

Quinn, W.H., Zopf, D.O., Short, K.S. and Kuo Yang, R.T.W. 1978. Historical trends and statistics of the southern oscillation, El Niño, and Indonesian droughts. *U.S. Fisheries Bulletin* 76: 663–678.

Philander, S.G. 1990. *El Niño, La Niña and the Southern Oscillation*. Academic, San Diego.

Pittock, A.B. 1984. On the reality, stability and usefulness of southern hemisphere teleconnections. *Australian Meteorological Magazine* 32(2): 75–82.

Reichl, P. 1976. The Riverine Plains of northern Victoria. In Holmes, J.H. (ed.) *Man and the Environment: Regional Perspectives*. Longman, Hawthorn, pp. 69–95.

Shove, D.J. 1987. Sunspot cycles. In Oliver, J.E. and Fairbridge, R.W. (eds) *Encyclopedia of Climatology*. Van Nostrand Reinhold, New York, pp. 807–815.

Stephenson, D.B. 1999. *The North Atlantic Oscillation thematic web site*. <http://www.met.rdg.ac.uk/cag/NAO/>

Trenberth, K.E. and Hurrell, J.W. 1994. Decadal atmospheric–ocean variations in the Pacific. *Climate Dynamics* 9: 303–319.

Tyson, P.D., Dyer, T.G.S., and Mametse, M.N. 1975. Secular changes in South African rainfall 1880–1972. *Quarterly Journal of the Royal Meteorological Society* 101: 817–833.

Villwock, A. 1998. *CLIVAR initial implementation plan: Chapter 5, The North Atlantic Oscillation*. <http://www.clivar.org/publications/other_pubs/iplan/iip/pd1.htm>

Wang, S-W. and Zhao, A-C. 1981. Droughts and floods in China 1440–1979. In Wigley, T.M.L., Ingram, M.J. and Farmer, G. (eds) *Climate and History, Studies in Past Climates and Their Impact on Man*. Cambridge University Press, Cambridge, pp. 271–288.